Effect of imperfections on the hyperuniformity of many-body systems

Jaeuk Kim and Salvatore Torquato

Phys. Rev. B **97**, 054105 — Published 12 February 2018

DOI: 10.1103/PhysRevB.97.054105

Effect of Imperfections on the Hyperuniformity of Many-Body Systems

Jaeuk Kim[1] and Salvatore Torquato[1, 2, 3, 4, *]

[1] *Department of Physics, Princeton University, Princeton, New Jersey 08544, USA*
[2] *Department of Chemistry, Princeton University, Princeton, New Jersey 08544, USA*
[3] *Princeton Institute for the Science and Technology of Materials, Princeton University, Princeton, New Jersey 08544, USA*
[4] *Program in Applied and Computational Mathematics, Princeton University, Princeton, New Jersey 08544, USA*

(Dated: January 25, 2018)

A hyperuniform many-body system is characterized by a structure factor $S(\boldsymbol{k})$ that vanishes in the small wavenumber limit, or equivalently by a local number variance $\sigma_N^2(R)$ associated with a spherical window of radius R that grows more slowly than R^d in the large-R limit. Thus, the hyperuniformity implies an anomalous suppression of long-wavelength density fluctuations relative to those in typical disordered systems, i.e., $\sigma_N^2(R) \sim R^d$ as $R \to \infty$. Hyperuniform systems include perfect crystals, quasicrystals, and special disordered systems. Disordered hyperuniform systems are amorphous states of matter that lie between a liquid and crystal [Torquato *et al.*, Phys. Rev. X, **5**, 021020, (2015)], and have been the subject of many recent investigations due to their novel properties. In the same way that there is no perfect crystal in practice due to the inevitable presence of imperfections, such as vacancies and dislocations, there is no "perfect" hyperuniform system, whether it is ordered or not. Thus, it is practically and theoretically important to quantitatively understand the extent to which imperfections introduced in a perfectly hyperuniform system can degrade or destroy its hyperuniformity and corresponding physical properties. This paper begins such a program by deriving explicit formulas for $S(\boldsymbol{k})$ in the small wavenumber regime for three types of imperfections: (1) uncorrelated point defects, including vacancies and interstitials, (2) stochastic particle displacements, and (3) thermal excitations in the classical harmonic regime. We demonstrate that our results are in excellent agreement with numerical simulations. We find that "uncorrelated" vacancies or interstitials destroy hyperuniformity in proportion to the defect concentration p. We show that "uncorrelated" stochastic displacements in lattices can never destroy the hyperuniformity but they can degrade hyperuniform systems into *class III* hyperuniform systems where $\sigma_N^2(R) \sim R^{d-\alpha}$ as $R \to \infty$ and $0 < \alpha < 1$. By contrast, we demonstrate that certain "correlated" displacements can make systems nonhyperuniform. For a perfect (ground-state) crystal at zero temperature, increase in temperature T introduces such correlated displacements resulting from thermal excitations, and thus the *thermalized crystal* becomes nonhyperuniform, even at an arbitrarily low temperature. It is noteworthy that imperfections in disordered hyperuniform systems can be unambiguously detected. Our work provides the theoretical underpinnings to systematically study the effect of imperfections on the physical properties of hyperuniform materials.

I. INTRODUCTION

Hyperuniform many-body systems in d-dimensional Euclidean space $\mathbb{R}^d$ are characterized by anomalously suppressed density fluctuations at large length scales, which can be quantified by a local number variance $\sigma_N^2(R)$ that grows more slowly than the window volume R^d in the large-window radius R limit. Equivalently, the hyperuniformity can be identified by a structure factor $S(\boldsymbol{k})$ that vanishes in the small-wavenumber limit, i.e., $\lim_{|\boldsymbol{k}|\to 0} S(\boldsymbol{k}) = 0$ [1–3]. The hyperuniformity concept provides a unified way to categorize crystals, quasicrystals [4, 5], and certain unusual disordered systems [1, 3, 6]. Disordered hyperuniform systems are ideal amorphous states of matter that lie between a crystal and liquid: they behave like perfect crystals in the manner in which they suppress large-scale density fluctuations and yet, like liquids and glasses, are statistically isotropic without Bragg peaks. In this sense, disordered hyperuniform systems have a hidden order on large length scales, which endows them with novel physical properties [7–13].

Over the last decade, there has been an increasing realization that disordered hyperuniform systems play a vital role in a number of problems in physics, mathematics, biological sciences, and engineering. For example, disordered hyperuniform systems exist as both equilibrium and non-equilibrium states, including disordered classical ground states [14–18], certain classical Coulomb plasmas [19–23], ground states of fermionic and bosonic systems [24–26], maximally random jammed (MRJ) hard-sphere packings [27–29], driven non-equilibrium systems [30–34], highly excited cold atoms [35], spatial patterns of photoreceptors in avian retina [36], novel disordered photonic materials [7, 8, 13], optimized patterns of pinning sites in type-II superconductors [11], transparent dense disordered materials [9], highly diffusive porous media [12], nearly optimal conducting two-phase media [37], and number theory [19, 38]. Recently, Torquato [39] has categorized hyperuniform systems into three classes: classes I, II, and III, which are defined by the large-R behavior of $\sigma_N^2(R)$, i.e., $\sigma_N^2(R) \sim R^{d-1}$, $\sigma_N^2(R) \sim R^{d-1} \ln R$, and $\sigma_N^2(R) \sim R^{d-\alpha}$ for $0 < \alpha < 1$, respectively.

It is well-known that imperfections play significant roles in determining physical and structural properties of crystals; see Refs. [40–42] and references therein. For instance, metallic crystals can be significantly hardened by increasing densities of point defects and dislocations, i.e., strain hardening [40, 43]. In semiconductors and insulators, impurities of certain elements can change their properties, such as electrical conductivities and colors [40, 41]. Another example is an anomalous phenomenon that the electrical resistivity of metal increases as the temperature drops below a certain value due to magnetic impurities, called the Kondo effect [44, 45].

Importantly, understanding how imperfections can affect the hyperuniformity of a system and its associated physical properties has been currently lacking for both ordered and disordered hyperuniform solid-phase systems. Our interest in this paper is to explore the degree to which the introduction of imperfections in perfectly ordered or disordered hyperuniform systems degrades or destroys their original perfect hyperuniformity. This is accomplished by quantifying the corresponding structure factors. Interestingly, the hyperuniformity concept provides a precise mathematical means of detecting imperfections in amorphous hyperuniform systems via either the violation of the hyperuniformity criterion, i.e., $\lim_{|\boldsymbol{k}|\to 0} S(\boldsymbol{k}) = 0$, or changes in the small-wavenumber behavior of $S(\boldsymbol{k})$. It is important to note that in the same way that there is no perfect ordered hyperuniform system (i.e., crystals and quasicrystals) in practice due to the inevitable existence of imperfections, such as point defects [40–42], dislocations [40–42], and phasons [46], there is no perfect disordered hyperuniform system.

It is instructive to discuss briefly computational and experimental methods that have been formulated to construct disordered hyperuniform systems. Computational methods have been developed in both equilibrium and nonequilibrium systems. For example, the collective-coordinate optimization technique is a computational tool that generates classical ground states with a target structure factor $S(\boldsymbol{k})$ for a set of wavevectors [14, 16–18, 47, 48]. Packing protocols such as Lubachevsky-Stillinger (LS) and Torquato-Jiao (TJ) algorithms are used to obtain (putative) strictly jammed MRJ hard-sphere packings, which are conjectured to be hyperuniform [1, 29, 49]. Random organization models [30, 34, 50, 51] can yield disordered hyperuniform point configurations at the critical point. Recently, Ma and Torquato demonstrated that the Cahn-Hilliard and Swift-Hohenberg equations can yield disordered hyperuniform scalar fields [52]. Experimental methods have been devised to produce (nearly) disordered hyperuniform systems, including periodically driven colloidal suspensions [31], jammed colloidal suspensions [53–55], annealed amorphous silicon [56], and self-assembling patterns of block-copolymers [57].

Such disordered hyperuniform systems, whether they are in thermal equilibrium or not, inevitably include some fraction of imperfections. Such imperfections may degrade or destroy the hyperuniformity, albeit in some cases to a small degree. For instance, any *compressible* system in thermal equilibrium, which has a positive isothermal compressibility ($\kappa_T > 0$), cannot be hyperuniform at positive temperatures due to thermal excitations. This conclusion follows from the *fluctuation-compressibility relation* [3, 16, 39], i.e., $S(\mathbf{0}) = \rho\kappa_T k_B T$, where ρ is number density, k_B is the Boltzmann constant, and T is the temperature. By theoretically estimating the isothermal compressibility of excited states at sufficiently low T associated with certain disordered hyperuniform ground states, Torquato *et al.* [16] utilized the aforementioned compressibility relation to quantify how hyperuniformity is destroyed in such cases. However, an understanding of the underlying mechanisms that result in the destruction of hyperuniformity for positive temperatures as well as the behavior of the structure factor away from the origin, whether the ground states are ordered or not, has heretofore been lacking.

It can be also difficult to generate perfect realizations of nonequilibrium hyperuniform systems, partly due to a type of *critical slowing down* phenomenon [39, 49]. This refers to the fact that such nonequilibrium systems are at critical points, which require significantly longer and longer computational times to achieve as the critical states are approached [29, 30, 33, 49, 50]. For instance, MRJ hard-sphere packings correspond to the hyperuniform critical states that occur at the jamming transition [29, 49]. Due to a critical slowing down as well as the presence of "rattlers" imperfections, numerically generated MRJ packings deviate from being perfectly strictly jammed and hence are not perfectly hyperuniform, e.g., $S(0) \sim 10^{-4}$ [29, 49]. It has been conjectured that the ideal MRJ state is free of any rattlers and hence would be exactly hyperuniform [1, 39].

Since imperfections as well as finite-size effects and numerical errors affect hyperuniformity of systems in computer simulations and experiments, it is desirable to develop a rough criterion to determine whether a system is "nearly" or "effectively" hyperuniform. A useful empirical and operational criterion that has been proposed [39, 49] for this purpose is the hyperuniform metric H, which is defined by

$$H \equiv \frac{S(\boldsymbol{k} \to \mathbf{0})}{S(\boldsymbol{k}_{\rm peak})}, \tag{1}$$

where $S(\boldsymbol{k}_{\rm peak})$ is the structure factor at the first dominant peak. A given disordered system can be regarded as effectively hyperuniform if the ratio H is of the order of 10^{-4} or smaller.

The overall objective of this paper is to understand quantitatively the extent to which hyperuniformity is degraded or destroyed when one introduces the following three types of imperfections into perfectly hyperuniform many-body systems: (1) uncorrelated point defects, including vacancies and interstitials, (2) stochastic particle displacements, and (3) thermal excitations. The left panel of Fig. 1 illustrates configurations of (a) a perfect

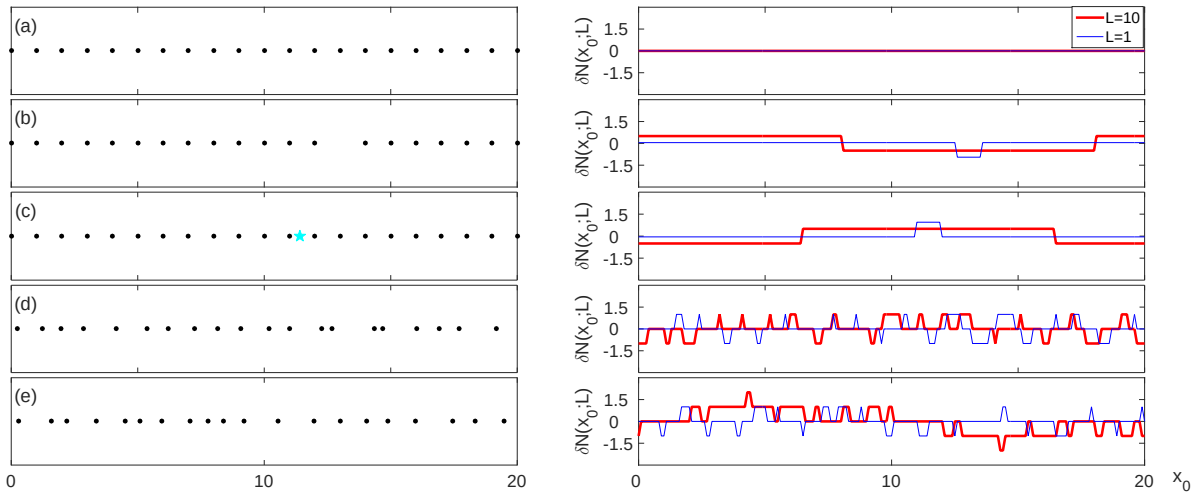

FIG. 1. (Color online) Left panel: Configurations of (a) an initially perfectly hyperuniform integer lattice and (b)-(e) imperfect lattices. The different types of imperfections include the following: (b) a single vacancy, (c) a single interstitial defect [denoted by a solid cyan five-pointed star], (d) uncorrelated stochastic particle displacements u via a uniform distribution with the variance $\langle u^2 \rangle = 0.05$, and (e) thermalized excitations, i.e., elastic waves at $\overline{T} = 0.05$, where $\overline{T}$ is a dimensionless temperature (54). Right panel: Corresponding deviations in the number of particles $N(x_0; L)$ inside a window centered at x_0, i.e., $\delta N(x_0; L) \equiv N(x_0; L) - \langle N(x_0; L) \rangle$ at two different window sizes L. The local number variance $\sigma_N^2(L)$, or equivalently the volume average of $\delta N(x_0; L)^2$, measures the degree of density fluctuations at a given length scale L. Roughly speaking, a system is nonhyperuniform if $\sigma_N^2(L)$ grows as the window size increases, as in cases (b), (c) and (d). By contrast, the perturbed system (d) is hyperuniform.

integer lattice and (b)-(e) four imperfect variants. While the integer lattice (a) is obviously hyperuniform, it is difficult to determine whether the others are hyperuniform with the naked eye.

Note that the right panel of Fig. 1 enables one to gauge qualitatively whether they are hyperuniform by looking at the deviation $\delta N(x_0; L)$ or the volume average of $\delta N(x_0; L)^2$, i.e., the local number variance $\sigma_N^2(L)$. We show that while in three systems (b), (c) and (e), density fluctuations are larger [i.e., the deviation $\delta N(x_0; L)$ becomes non-zero more frequently] at the larger length scales ($L = 10$) than at the smaller ones ($L = 1$), the density fluctuations in (d) barely change with length scales. This observation qualitatively shows that the imperfect system described in (d) is hyperuniform, but the others in (b), (c) and (e) are not, although counterintuitively the particles in (d) look more clustered than those in (e). The nonhyperuniformity of the example in (e) can be qualitatively understood by noting that thermalized excitations in a crystal can be decomposed into a sum of sinusoidal functions with different wavelengths. A single longitudinal lattice wave of the longest wavelength induces global inhomogeneity with density modulation in which one half of the system becomes denser than the other half of the system, and hence results in nonhyperuniformity.

In the main text, we will quantitatively validate all of these qualitative explanations by deriving explicit formulas for $S(\boldsymbol{k})$ in the small-$|\boldsymbol{k}|$ regime for each type of imperfection. We then demonstrate that our theoretical results are in excellent agreement with corresponding numerical simulations.

We begin by showing that uncorrelated point defects (both vacancies and interstitials) destroy the hyperuniformity in proportion to the defect concentration p for small p. While we focus in this context on two types of point defects, these results can be easily generalized to other types of point defects. Subsequently, we quantitatively study *perturbed point processes* [58–60], which are generated from an initial point process by stochastically displacing each point in either an uncorrelated or correlated manner. When displacements are uncorrelated, although the hyperuniformity is degraded to some extent, it is never destroyed, i.e., still $\lim_{|\boldsymbol{k}| \to 0} S(\boldsymbol{k}) = 0$. Using this property, we present a simple method that transforms class I systems (e.g., lattices and disordered stealthy hyperuniform systems) to class III systems [39]; see Eq. (12). In addition, we ascertain conditions under which stochastic displacements can destroy the hyperuniformity of initial hyperuniform point processes, both ordered and disordered.

This study is followed by an investigation of *thermalized crystals*, i.e., classical crystals in thermal equilibrium in the harmonic regime. Due to thermal motions, particles in a thermalized crystal are displaced from their ideal arrangement, i.e., a ground-state crystal. At first glance, one might think that at a sufficiently low temperature, a thermalized crystal is the same as an uncorrelated perturbed lattice, and thus it is hyperuniform. However, this picture is wrong because excited particles move collectively and form long-wavelength lattice waves. We prove

that thermalized crystals can be mapped to special correlated perturbed lattices that are "nonhyperuniform." We show that our expression for $S(\boldsymbol{k})$ are in excellent agreement with numerical simulations at temperatures much lower than the melting point [61]. Our expression for $S(\boldsymbol{k})$ in the zero-wavenumber limit also yields the correct isothermal compressibility κ_T in the low temperature limit.

We present basic mathematical definitions and concepts in Sec. II. In Sec. III, we theoretically and numerically investigate effects of uncorrelated point defects on the hyperuniformity of otherwise hyperuniform systems. In Sec. IV, we study the hyperuniformity of perturbed point processes. Here, we introduce and examine a family of singlet displacement probability densities to generate class III systems [39]. In Sec. V, we investigate effects of thermal excitations in classical harmonic lattices on their hyperuniformity. Finally, we provide concluding remarks in Sec. VI.

II. BASIC DEFINITIONS AND CONCEPTS

A. Point processes

Roughly speaking, a point process in d-dimensional Euclidean space $\mathbb{R}^d$ is a spatial distribution of infinitely many points $\boldsymbol{x}_1,\ \boldsymbol{x}_2,\ \cdots$, in $\mathbb{R}^d$, which can be described by a microscopic density function $n(\boldsymbol{r})$:

$$n(\boldsymbol{r}) = \sum_{i=1}^{\infty} \delta(\boldsymbol{r} - \boldsymbol{x}_i)\,, \tag{2}$$

where $\delta(\boldsymbol{x})$ denotes the Dirac delta function in $\mathbb{R}^d$. The n-point density correlation function $\rho_n(\boldsymbol{r}^n)$ is defined by $\rho_n(\boldsymbol{r}^n) \equiv \langle n(\boldsymbol{r}_1)\, n(\boldsymbol{r}_2) \cdots n(\boldsymbol{r}_n)\rangle$, where $\boldsymbol{r}^n = \boldsymbol{r}_1, \boldsymbol{r}_2, \cdots, \boldsymbol{r}_n$ and $\langle\cdot\rangle$ represents an ensemble average. This function is proportional to the probability density associated with finding n different points at $\boldsymbol{r}_1, \boldsymbol{r}_2, \cdots, \boldsymbol{r}_n$. For statistically homogeneous point processes at a given number density ρ (number of particles per unit volume), the n-point correlation function depends on relative positions of points, i.e., $\rho_n(\boldsymbol{r}^n) = \rho^n\, g_n(\boldsymbol{r}_{21}, \cdots, \boldsymbol{r}_{n1})$ with $\boldsymbol{r}_{ij} \equiv \boldsymbol{r}_j - \boldsymbol{r}_i$ for $1 \le i \ne j \le n$ and $\rho_1(\boldsymbol{r}) = \rho$.

The *pair correlation function* $g_2(\boldsymbol{r})$ and *total correlation function* $h(\boldsymbol{r})$, defined as $h(\boldsymbol{r}) \equiv g_2(\boldsymbol{r}) - 1$, are of special importance in statistical mechanics [62]. For systems without long-range order, $g_2(\boldsymbol{r}) \to 1$ and $h(\boldsymbol{r}) \to 0$ as $|\boldsymbol{r}| \to \infty$. The *autocovariance function* $\chi(\boldsymbol{r}) \equiv \langle [n(\boldsymbol{r} + \boldsymbol{r}_0) - \rho]\, [n(\boldsymbol{r}_0) - \rho]\rangle$ is related to $h(\boldsymbol{r})$ via

$$\chi(\boldsymbol{r}) = \rho\, [\delta(\boldsymbol{r}) + \rho\, h(\boldsymbol{r})]\,. \tag{3}$$

B. Structure Factor

The *static structure factor* is a mathematical description of scattering intensities. For a finite point configuration $\{\boldsymbol{x}_i\}_{i=1}^N$ of N particles in a unit cell of volume V, the static structure factor is defined as

$$\mathcal{S}(\boldsymbol{k}) \equiv \frac{1}{N}\,|\tilde{n}(\boldsymbol{k})|^2 = 1 + \frac{1}{N}\sum_{i\ne j=1}^{N} \exp(-i\boldsymbol{k}\cdot(\boldsymbol{x}_i - \boldsymbol{x}_j)), \tag{4}$$

where the *collective coordinates* $\tilde{n}(\boldsymbol{k})$ is the Fourier transform of the microscopic density $n(\boldsymbol{r})$. Under periodic boundary conditions, wavevectors $\boldsymbol{k}$ are constrained to lie on reciprocal lattice vectors of the unit cell, satisfying $\exp(i\boldsymbol{k}\cdot\boldsymbol{a}_j) = 1$ for all basis vectors $\boldsymbol{a}_j$ of the unit cell. Thus, in the thermodynamic limit ($N \to \infty$ with $\rho \equiv N/V$ fixed), a wavevector $\boldsymbol{k}$ becomes a continuous parameter.

In the thermodynamic limit, the static structure factor of a point process is defined by an ensemble average $\langle \mathcal{S}(\boldsymbol{k})\rangle$ of (4) with the forward scattering excluded:

$$S(\boldsymbol{k}) \equiv \langle \mathcal{S}(\boldsymbol{k})\rangle - (2\pi)^d \rho\, \delta(\boldsymbol{k}). \tag{5}$$

The static structure factor (5) is related to the Fourier transform of two-point functions, $h(\boldsymbol{r})$ and $\chi(\boldsymbol{r})$, defined in the expression (3): $S(\boldsymbol{k}) = 1 + \rho\,\tilde{h}(\boldsymbol{k}) = \tilde{\chi}(\boldsymbol{k})\,/\rho$. In the rest of this paper, unless otherwise stated, $S(\boldsymbol{k})$ denotes the static structure factors defined in (5).

We will use the following definition of Fourier transform $\tilde{f}(\boldsymbol{k})$ and the inverse transform $f(\boldsymbol{r})$ (assuming their existence):

$$\tilde{f}(\boldsymbol{k}) = \int_{\mathbb{R}^d} f(\boldsymbol{r})\, e^{-i\boldsymbol{k}\cdot\boldsymbol{r}}\, d\boldsymbol{r}\,, \tag{6}$$

$$f(\boldsymbol{r}) = \left(\frac{1}{2\pi}\right)^d \int_{\mathbb{R}^d} \tilde{f}(\boldsymbol{k})\, e^{i\boldsymbol{k}\cdot\boldsymbol{r}}\, d\boldsymbol{k}\,. \tag{7}$$

C. Hyperuniformity

Consider a statistically homogeneous point process at number density ρ in d-dimensional Euclidean space $\mathbb{R}^d$. Hyperuniform [1, 3] (also known as 'superhomogeneous' [63]) point processes are ones in which long-wavelength density fluctuations are suppressed. Quantitatively, hyperuniformity can be defined in Fourier space via

$$\lim_{|\boldsymbol{k}|\to 0} S(\boldsymbol{k}) = 0, \tag{8}$$

or, alternatively, in direct-space via the *local number variance* $\sigma_N^2(R)$:

$$\lim_{v_1(R)\to\infty} \frac{\sigma_N^2(R)}{v_1(R)} = 0, \tag{9}$$

where $v_1(R)$ is the volume of a d-dimensional hypersphere of radius R. Here, the local number variance $\sigma_N^2(R)$ represents the variance in the number of points sampled by randomly placed spherical windows of radius R (see Fig.

1), which can be calculated from the following relations [1, 39]:

$$\sigma_N^2(R) = \rho\, v_1(R) \left[1 + \rho \int_{\mathbb{R}^d} d\boldsymbol{r}\, h(\boldsymbol{r})\, \alpha_2(\boldsymbol{r}; R)\right] \tag{10}$$

$$= \frac{\rho\, v_1(R)}{(2\pi)^d} \int_{\mathbb{R}^d} d\boldsymbol{k}\, S(\boldsymbol{k})\, \tilde{\alpha}_2(\boldsymbol{k}; R)\,, \tag{11}$$

where $\alpha_2(\boldsymbol{r}; R)$ represents the scaled intersection volume of two spherical windows of radius R that are separated by $\boldsymbol{r}$, and $\tilde{\alpha}_2(\boldsymbol{k}; R)$ is its Fourier transform.

Consider hyperuniform systems that are characterized by structure factors with power-law form for small wavenumbers; $S(\boldsymbol{k}) \sim |\boldsymbol{k}|^\alpha$. The exponent α determines the large-R asymptotic behavior of $\sigma_N^2(R)$ [1–3]. Using this asymptotic behavior, Torquato recently has categorized hyperuniform point processes into three classes [39]:

$$\sigma_N^2(R) \sim \begin{cases} R^{d-1}, & \alpha > 1 \quad \text{(class I)} \\ R^{d-1} \ln(R)\,, & \alpha = 1 \quad \text{(class II)} \\ R^{d-\alpha}, & 0 < \alpha < 1 \quad \text{(class III).} \end{cases} \tag{12}$$

Class I systems include crystals, some quasicrystals, and *disordered stealthy hyperuniform* systems [1, 2, 16, 17]. A variety of examples of class II and III systems are given in Ref. [39].

Stealthy hyperuniform ground-state systems are defined by the condition that $S(\boldsymbol{k}) = 0$ for $0 \le |\boldsymbol{k}| < K$ for some positive number K. The parameter χ provides a measure of the relative fraction of the number of wavevectors at which $S(\boldsymbol{k})$ is constrained to be zero to the total number of degrees of freedom [16, 39]. For $0 < \chi < 1/2$, the entropically favored stealthy hyperuniform ground states are highly degenerate and disordered, while they crystallize for $1/2 < \chi \le 1$.

For single-component systems in thermal equilibrium, the *fluctuation-compressibility relation* is given by [62]

$$\lim_{|\boldsymbol{k}|\to 0} S(\boldsymbol{k}) = \rho \kappa_T k_B T, \tag{13}$$

where κ_T is the isothermal compressibility, and T is the temperature of the system. Since the left-hand side of (13) is directly related to the long-wavelength density fluctuations, i.e., $S(\boldsymbol{0}) = \lim_{R\to\infty} \sigma_N^2(R)/(\rho\, v_1(R))$, any compressible system in thermal equilibrium ($\kappa_T > 0$) cannot be hyperuniform at a positive T; see Refs. [16] and [39] for more discussion on this subject.

III. EFFECT OF SPATIALLY UNCORRELATED DEFECTS

The dimensionality of spatial distribution of imperfections enables a classification into four types: point, line, surface, and volume defects. Roughly speaking, three types of point defects can be considered; vacancies (missing atoms), interstitial impurities (excess atoms) and substitutional impurities (different kinds of atoms). Dislocations and stacking faults are examples of line and surface defects, respectively. Volume defects include pores and cracks.

Some theories have been devised to identify types and amount of point defects in crystalline solids via existing experimental techniques such as EPR and X-ray scattering experiments [64, 65]. For instance of scattering experiments, one can determine types and sizes of point defects, and whether they are isolated or aggregated, by analyzing the shifts of Bragg peaks and asymmetric diffuse scattering around the Bragg peaks called *Huang diffuse scattering* [66, 67].

In this section, we investigate how the introduction of *uncorrelated* point defects influences hyperuniformity of an original hyperuniform point process at number density ρ. Here, we consider a d-dimensional hyperuniform point configuration $\{\boldsymbol{r}_i\}_{i=1}^{N_s}$ in a periodic unit cell of volume V, and two types of point defects; (1) vacancies and (2) interstitials. The structure factor of this original configuration is denoted by $S_0(\boldsymbol{k})$. For the simplicity, we do not consider elastic deformations in imperfect configurations due to defects, which can arise in Huang diffuse scattering [66, 67], as well as steric repulsion that can restrict the interstitial positions.

A. Point Vacancies

Here, we consider spatially uncorrelated point vacancies by independently removing particles in original configurations. Let us define a stochastic function $f(\boldsymbol{r})$ to describe point defects in $\mathbb{R}^d$. In general, $f(\boldsymbol{r})$ is complex-valued, but for uncorrelated point vacancies, it becomes real-valued such that

$$\Pr(f(\boldsymbol{r}) = a) = \begin{cases} 1-p, & \text{if } a = 1 \\ p, & \text{if } a = 0, \end{cases} \tag{14}$$

where p is the concentration of vacancies. After introducing uncorrelated point vacancies, one can express the structure factor of a defective configuration in terms of the function $f(\boldsymbol{r})$;

$$\mathcal{S}(\boldsymbol{k}) = 1 + \left\langle \frac{1}{\mathcal{N}} \sum_{i\neq j=1}^{N_s} f_i {f_j}^* e^{-i\boldsymbol{k}\cdot(\boldsymbol{r}_i - \boldsymbol{r}_j)} \right\rangle_f, \tag{15}$$

where f_i is an abbreviation of $f(\boldsymbol{r}_i)$, ${f_i}^*$ is its complex conjugate, $\langle\cdot\rangle_f$ represents the expectation value over $f(\boldsymbol{r})$. Here, $\mathcal{N} \equiv \sum_{i=1}^{N_s} f_i$ is the number of remaining particles in the configuration, which is a random variable that follows the binomial distribution:

$$\Pr(\mathcal{N} = N) = \binom{N_s}{N} (1-p)^N p^{N_s - N}, \tag{16}$$

and its expectation value is $\langle\mathcal{N}\rangle_f = (1-p)N_s$.

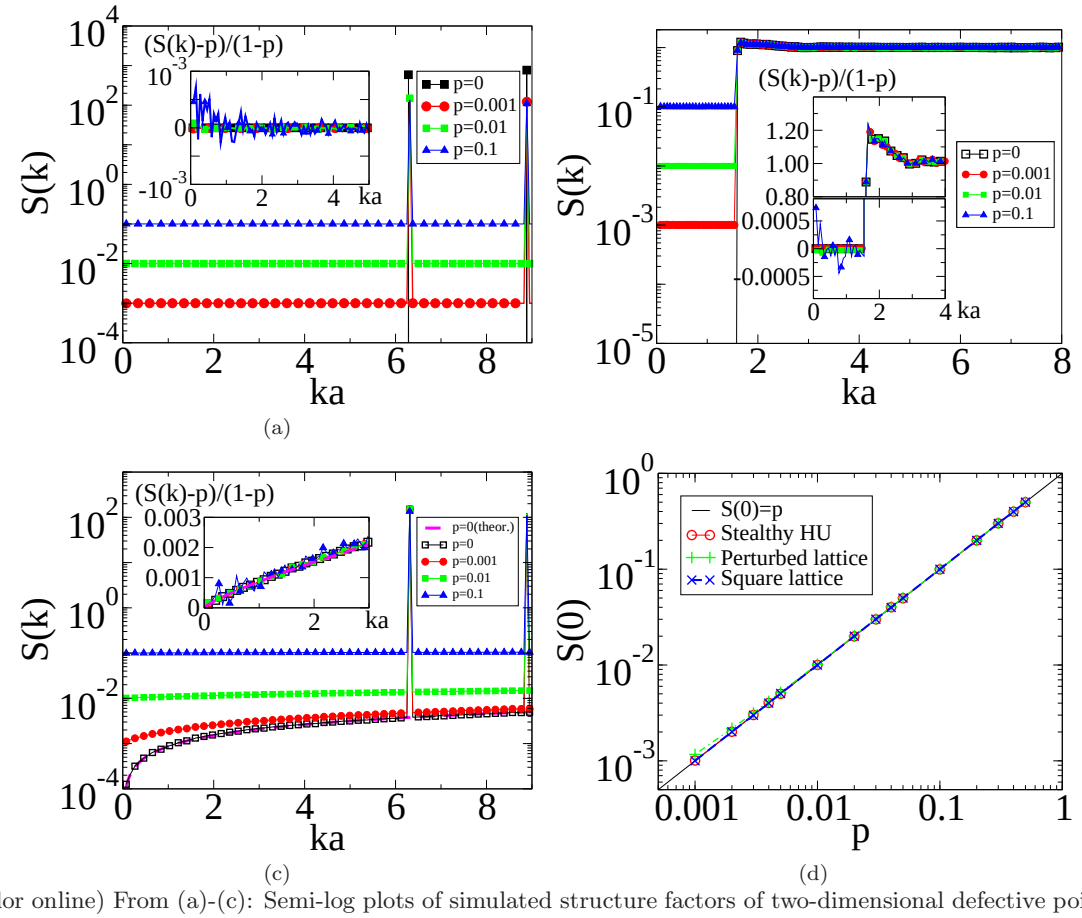

FIG. 2. (Color online) From (a)-(c): Semi-log plots of simulated structure factors of two-dimensional defective point configurations with point vacancies of the fraction p. Three types of original configurations include (a) the square lattice, (b) stealthy disordered hyperuniform configurations with $\chi = 0.1$, and (c) perturbed square lattices via a distribution $f_1(\boldsymbol{u}; \delta = 10^{-4}, \alpha = 0.8)$ given by (35). In (c), theoretical values of $S_0(k)$ for perturbed lattices (magenta dashed line) are calculated from (36). Insets of each panel zoom into the small-wavenumber regime in linear scale, but y-axes are rescaled as $(S(k) - p)/(1 - p)$. Note that peaks observed in (a) and (c) correspond to the first two Bragg peaks of the square lattice. Subfigure (d) is comparison of the prediction (20) to corresponding computer simulations of $S(0)$ of defective systems as functions of the vacancy concentration p for three original systems.

One can alternatively express the expectation in (15) as

$$\left\langle \frac{1}{\mathcal{N}} \sum_{i\neq j=1}^{N_s} f_i f_j e^{-i\boldsymbol{k}\cdot(\boldsymbol{r}_i-\boldsymbol{r}_j)} \right\rangle_f$$
$$= \sum_{N=0}^{N_s} \Pr(\mathcal{N}=N) \frac{1}{N} \sum_{i\neq j=1}^{N_s} \langle f_i f_j \rangle_N \, e^{-i\boldsymbol{k}\cdot(\boldsymbol{r}_i-\boldsymbol{r}_j)} \quad (17)$$
$$= (1-p)\frac{1}{N_s} \sum_{i\neq j=1}^{N_s} e^{-i\boldsymbol{k}\cdot(\boldsymbol{r}_i-\boldsymbol{r}_j)}, \quad (18)$$

where the conditional expectation value of $f_i f_j$ when $\mathcal{N} = N$ is given by

$$\langle f_i f_j \rangle_N = \frac{N(N-1)}{{N_s}^2} = \left(\frac{N}{N_s}\right)^2 + \mathcal{O}({N_s}^{-1}), \quad (19)$$

where $\mathcal{O}(f(x))$ means that its value is smaller than $a\, f(x)$ for some positive constant a as x increases. Substituting Eqs. (16) and (19) into Eq. (17) yields the result (18), and thus, the structure factor (15) of the defective point process in any space dimension is given by

$$S(\boldsymbol{k}) = 1 + (1-p)\frac{1}{N_s}\left\langle \sum_{i\neq j=1}^{N_s} e^{i\boldsymbol{k}\cdot(\boldsymbol{r}_i-\boldsymbol{r}_j)} \right\rangle$$
$$= 1 + (1-p)(S_0(\boldsymbol{k}) - 1)$$
$$= p + (1-p)\, S_0(\boldsymbol{k}). \quad (20)$$

This result was previosuly known for defective crystals [65, 66].

We note that Eq. (20) is valid for any original point configuration whether it is hyperuniform or not. Formula (20) implies that the rescaled the structure factor as $[S(\boldsymbol{k}) - p]/(1-p)$ yields the structure factor $S_0(\boldsymbol{k})$ of the original system, regardless of the vacancy concentration p. Using this rescaling idea in insets in Fig. 2, we show that numerical simulations are in excellent agreement with our theoretical prediction (20). Application

of the effective hyperuniformity criterion (1) to the imperfect disordered systems described in Fig. 2 (b) shows that their hyperuniformity metric H is of the same order of p (i.e., $H_{\text{vacancies}} \sim p$), and thus they cannot be regarded as effectively hyperuniform whenever $p > 10^{-4}$.

Using Eqs. (20) and (11), the *local number variance* $\sigma_N^2(R;p)$ of a point process in $\mathbb{R}^d$ with the vacancy concentration p is straightforwardly obtained as

$$\sigma_N^2(R;p) = (1-p)p\rho\, v_1(R) + (1-p)^2\, \sigma_N^2(R;0)\,, \quad (21)$$

where ρ is number density of the initial point process. Note that the first term in Eq. (21) corresponds to variance in the number of vacancies inside a spherical window. Thus, the nonhyperuniformity due to uncorrelated point vacancies is attributed to the tendency of vacancies to cluster, as in Poisson point processes. This result is consistent with an expression derived by Chieco *et al.* [68] for the related volume-fraction variance of two-dimensional square lattices with uncorrelated vacancies.

Remarks:

1. In the limit of $p \to 1$, $S(\boldsymbol{k}) \to 1$, which implies that the system behaves like the ideal gas regardless of the initial configuration.

2. To treat the case of substitutional impurities, one need to replace the random function $f(\boldsymbol{r})$ in Eq. (15) with the following expression;

$$[1 - f(\boldsymbol{r})]\, a_0(\boldsymbol{k}) + f(\boldsymbol{r})\, a_s(\boldsymbol{k})\,, \quad (22)$$

   where $a_0(\boldsymbol{k})$ and $a_s(\boldsymbol{k})$ are the scattering amplitude of a dominant atom and an impurity atom, respectively. Here, $f(\boldsymbol{r})$ is identical to the random function (14), but now its expectation value p stands for the concentration of the substitutional impurities.

3. In Fig. 2, we generate 100 independent initial configurations of $N_s = 10^4$ for each type of two-dimensional systems, which correspond to the case $p = 0$. In order to generate stealthy hyperuniform systems, we use the collective coordinate optimization technique described in Refs. [14] and [17]. From these initial configurations, for a given $p(\neq 0)$, we generate 10000 defective configurations by randomly removing n particles, where n is a random variable following the Poisson distribution with a mean pN_s. In Fig. 2(d), $S(0)$ represents an average of $S(k)$ at the three lowest wavenumbers.

B. Point Interstitials

Here, we consider spatially uncorrelated interstitials by independently adding particles in original perfectly hyperuniform configurations in $\mathbb{R}^d$. Suppose that the original configuration has N_s particles at number density ρ, and pN_s interstitials are introduced into the configuration. Thus, number density of a defective system becomes $(1+p)\rho$. Separating the collective coordinate $\tilde{n}(\boldsymbol{k})$ of a defective system into those of the original system and the interstitials, $\tilde{n}_0(\boldsymbol{k})$ and $\tilde{n}_I(\boldsymbol{k})$, the structure factor of the defective system can be written as

$$\begin{aligned} S(\boldsymbol{k}) &= \frac{1}{(1+p)N_s}\left\langle \left|\tilde{n}_0(\boldsymbol{k}) + \tilde{n}_I(\boldsymbol{k})\right|^2 \right\rangle \\ &\approx \frac{1}{(1+p)N_s}\left[\left\langle \left|\tilde{n}_0(\boldsymbol{k})\right|^2 \right\rangle + \left\langle \left|\tilde{n}_I(\boldsymbol{k})\right|^2 \right\rangle\right] \quad (23) \\ &= \frac{1}{1+p}\, S_0(\boldsymbol{k}) + \frac{p}{1+p}\, S_I(\boldsymbol{k})\,, \quad (24) \end{aligned}$$

where an approximation $\langle \tilde{n}_0(\boldsymbol{k})\, \tilde{n}_I(-\boldsymbol{k})\rangle \approx 0$ is used under the assumption that interstitials are uncorrelated with respect to the original systems. Here, the structure factor of interstitials is denoted by $S_I(\boldsymbol{k}) \equiv \left\langle \left|\tilde{n}_I(\boldsymbol{k})\right|^2 \right\rangle / (pN_s)$.

When the interstitial positions are completely uncorrelated (i.e., $S_I(\boldsymbol{k}) \to 1$), Eq. (24) can be simplified as

$$S(\boldsymbol{k}) = \frac{p}{1+p} + \frac{1}{1+p}\, S_0(\boldsymbol{k})\,. \quad (25)$$

We note that as like Eq. (20), Eq. (25) is valid for any original configuration whether it is hyperuniform or not, and in any space dimension d. For instance, if an original configuration is a Poisson point configuration [$S_0(\boldsymbol{k}) = 1$], then the defective configuration obviously becomes another Poisson point configuration at a different number density, i.e., $S(\boldsymbol{k}) = S_0(\boldsymbol{k})$.

For computer simulations, we consider only in one-dimension for simplicity; corresponding results for higher dimensions will not change qualitatively. Figure 3 compares the predictions of Eq. (25) to numerical simulations of one-dimensional (entropically-favored) stealthy hyperuniform ground states [16, 17] with $\chi = 0.3$, $K = 1$, and $N_s = 10^3$. For each of 100 original configurations, we generated 100 defective configurations by randomly adding m particles, where m is a random number chosen from the Poisson distribution with a mean pN_s. According to the effective hyperuniformity criterion (1), the imperfect disordered systems described in Fig. 3 are definitively not hyperuniform ($H_{\text{interstitials}} \sim p > 10^{-4}$). Figure 3 shows that Eq. (25) can provide a good approximation, even for large values of p.

Using Eqs. (11) and (25), one obtains an expression for the local number variance in the presence of uncorrelated interstitials as follows:

$$\sigma_N^2(R;p) = p\rho\, v_1(R) + \sigma_N^2(R;0)\,, \quad (26)$$

where p is the fraction of interstitials and ρ is the number density of the original system. Since the first term in Eq. (26) corresponds to the number variance of a Poisson point process at number density $p\rho$, the nonhyperuniformity of the defective systems is attributed to the tendency of the defects to cluster, which also occurs in a Poisson point process.

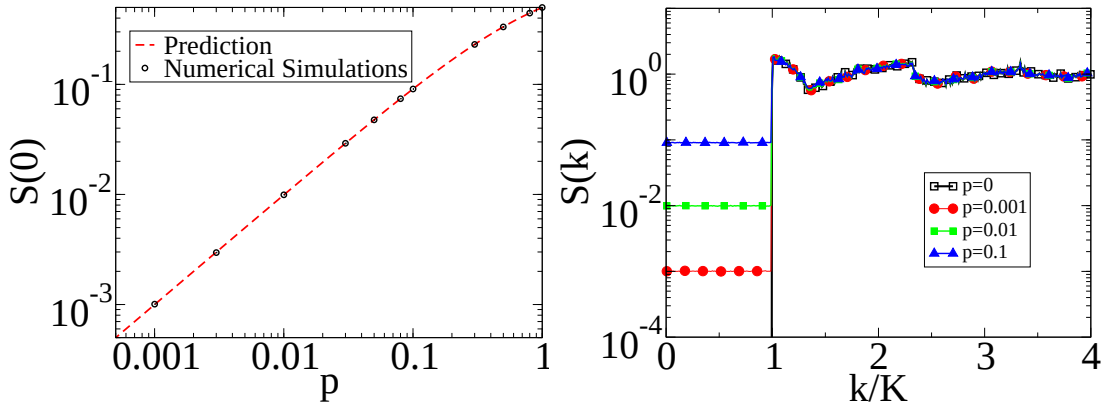

FIG. 3. Left panel: Comparison of the predictions of Eq. (25) to the corresponding computer simulations of $S(0)$ of the defective configurations with the fraction p of interstitials. Right panel: Semi-log plot of numerical results for the structure factor of defective point configurations with uncorrelated interstitials. The original perfectly hyperuniform systems are taken to be one-dimensional stealthy hyperuniform ground states with $\chi = 0.3$ and $K = 1$.

IV. EFFECT OF STOCHASTIC PARTICLE DISPLACEMENTS

We consider a *perturbed point process*, in which the position of ith particle in an initial point process is stochastically displaced from $\boldsymbol{r}_i$ to $\boldsymbol{r}_i + \boldsymbol{u}(\boldsymbol{r}_i)$, where $i = 1, 2, \cdots$. When the initial point process is a lattice, the perturbed system is referred to a *perturbed lattice* [58, 60] (also known as 'shuffled lattice' [1, 69]). Perturbed lattices have been studied or used in various contexts, including models of lattice disorders [58, 70], and subjects in probability theory, such as distribution of zeros of random entire functions [71] and number rigidity [72, 73]. Moreover, perturbed lattices are used to generate disordered initial configurations for numerical simulations [74], configurations of sampling points [75], and disordered hyperuniform point configurations [11, 76]. Here, we start with summary of results in the previous studies.

A. General Properties of Perturbed Point Processes

In the rest of this section, we consider a hyperuniform point process $\{\boldsymbol{r}_i\}_{i=1}^{\infty}$ at number density ρ in $\mathbb{R}^d$, and its structure factor and pair-correlation function are denoted by $S_0(\boldsymbol{k})$ and $g_2^{(0)}(\boldsymbol{r})$, respectively. For the simplicity, in the rest of this section, we assume that the stochastic displacement vectors $\boldsymbol{u}(\boldsymbol{r})$ follow an identical and isotropic singlet probability density function $f_1(\boldsymbol{u})$, and thus $\langle \boldsymbol{u} \rangle = \boldsymbol{0}$.

The structure factor of a perturbed point process depends on the initial point process and statistical properties of displacements [58, 60]:

$$S(\boldsymbol{k}) = 1 + \rho \int d\boldsymbol{r}\, e^{-i\boldsymbol{k}\cdot\boldsymbol{r}}\, g_2^{(0)}(\boldsymbol{r})\, \hat{\phi}(\boldsymbol{k};\boldsymbol{r})\,, \tag{27}$$

where $\hat{\phi}(\boldsymbol{k};\boldsymbol{r}) \equiv \int d\boldsymbol{u}\, d\boldsymbol{v} \exp(-i\boldsymbol{k}\cdot(\boldsymbol{u}-\boldsymbol{v}))\, f_2(\boldsymbol{u},\boldsymbol{v};\boldsymbol{r})$, and $f_2(\boldsymbol{u},\boldsymbol{v};\boldsymbol{r})$ stands for a conditional joint probability density function that two particles, separated by $\boldsymbol{r}$ in the initial point process, are displaced by $\boldsymbol{u}$ and $\boldsymbol{v}$, respectively.

If displacements of distinct particles are *uncorrelated*, then the joint probability density function can be reduced into a product of two singlet probability densities $f_1(\boldsymbol{u})$ and $f_1(\boldsymbol{v})$, i.e., $f_2(\boldsymbol{u},\boldsymbol{v};\boldsymbol{r}) = f_1(\boldsymbol{u})\, f_1(\boldsymbol{v})$, where $f_1(\boldsymbol{u})$ is the singlet probability density function of a displacement vector $\boldsymbol{u}$. Thus, the structure factor (27) of a perturbed point process with uncorrelated displacements is simply expressed by [59, 60]

$$S(\boldsymbol{k}) = \left(1 - \left|\tilde{f}_1(\boldsymbol{k})\right|^2\right) + \left|\tilde{f}_1(\boldsymbol{k})\right|^2 S_0(\boldsymbol{k})\,, \tag{28}$$

where $\hat{\phi}(\boldsymbol{k};\boldsymbol{r}) = \left|\tilde{f}_1(\boldsymbol{k})\right|^2$ and $\tilde{f}_1(\boldsymbol{k})$ is the characteristic function, or equivalently the Fourier transform, of $f_1(\boldsymbol{u})$. In contrast to the effect of point defects described in Sec. III, "uncorrelated" displacements cannot destroy the hyperuniformity of an original hyperuniform point process because $\tilde{f}_1(\boldsymbol{k} = \boldsymbol{0}) = 1$ by definition.

Suppose that the singlet probability density can be approximated by $f_1(\boldsymbol{u}) \approx A\,|\boldsymbol{u}|^{-(d+\gamma)}$ for large $|\boldsymbol{u}|$, and thus the small-wavenumber behavior of $\tilde{f}_1(\boldsymbol{k})$ depends on the exponent γ [60];

$$\tilde{f}_1(\boldsymbol{k}) \approx 1 - B_\gamma\, |\boldsymbol{k}|^{\min\{2,\gamma\}} \qquad (|\boldsymbol{k}| \ll 1), \tag{29}$$

where $\langle \boldsymbol{u} \rangle = \boldsymbol{0}$, $\min C$ represents the smallest element of a set C, and the coefficient B_γ is written as

$$B_\gamma = \begin{cases} \frac{1}{2d}\left\langle |\boldsymbol{u}|^2 \right\rangle, & \gamma > 2 \\ A(2\pi)^{d/2} \int_0^\infty dx\, \frac{J_{d/2-1}(x)}{x^{(d/2+\gamma)}}, & 0 < \gamma \le 2. \end{cases} \tag{30}$$

If $S_0(\boldsymbol{k}) \sim |\boldsymbol{k}|^\alpha$ for small $|\boldsymbol{k}|$, then the structure factor (28) of a perturbed point process is approximately given

as

$$S(\boldsymbol{k}) \sim |\boldsymbol{k}|^{\min\{2,\gamma,\alpha\}} \qquad (|\boldsymbol{k}| \ll 1). \tag{31}$$

Thus, an uncorrelated perturbed point process can belong to any class of hyperuniformity, i.e., classes I, II, and III [39], as long as the growth rate of its local number variance $\sigma_N^2(R)$ is faster than or equal to that of the original hyperuniform system.

For instance of one-dimensional perturbed lattice, if $f_1(\boldsymbol{u})$ has a finite variance, e.g., Gaussian distribution, the system always belongs to class I. Using the Cauchy distribution ($\gamma = 1$) [77] and the Pareto distribution ($\gamma < 1$) [78] as $f_1(\boldsymbol{u})$, one obtains class II [79] and class III perturbed lattices, respectively. However, it is impossible to change a class II system ($\alpha = 1$) to a class I system ($\alpha > 1$) via the uncorrelated stochastic displacements.

Now we consider cases of *correlated* displacements. Assuming that a displacement vector $\boldsymbol{u}$ is isotropically distributed and its variance $\left\langle |\boldsymbol{u}|^2 \right\rangle$ exists, $\hat{\phi}(\boldsymbol{k};\boldsymbol{r})$ in Eq. (27) can be expanded as a Taylor series of $\boldsymbol{k}$ for small $|\boldsymbol{k}|$ [60]:

$$\hat{\phi}(\boldsymbol{k};\boldsymbol{r}) = 1 + \sum_{\mu,\nu=1}^{d} k_\mu k_\nu \left[G_{\mu\nu}(\boldsymbol{r}) - G_{\mu\nu}(\boldsymbol{0})\right] + \mathcal{O}\Big(|\boldsymbol{k}|^4\Big), \tag{32}$$

where the *displacement-displacement correlation function* is defined as $G_{\mu\nu}(\boldsymbol{r}) \equiv \langle u_\mu(\boldsymbol{r}+\boldsymbol{r}_0) u_\nu(\boldsymbol{r}_0)\rangle$. For the simplicity, if we assume that two orthogonal components of displacements are uncorrelated when $d \geq 2$, which implies that $G_{\mu\nu}(\boldsymbol{r}) = \delta_{\mu\nu}\, G(\boldsymbol{r})$, then the general expression for the structure factor (27) can be approximated by for small wavenumbers [60];

$$\begin{aligned} S(\boldsymbol{k}) \approx{}& \Big[\, |\boldsymbol{k}|^2 G(\boldsymbol{0}) + \Big(1 - |\boldsymbol{k}|^2 G(\boldsymbol{0})\Big) S_0(\boldsymbol{k}) \,\Big] \\ &+ \rho\, |\boldsymbol{k}|^2 \left(\tilde{G}(\boldsymbol{k}) + \int d\boldsymbol{r}\, h_0(\boldsymbol{r})\, G(\boldsymbol{r})\, e^{-i\boldsymbol{k}\cdot\boldsymbol{r}} \right), \end{aligned} \tag{33}$$

where $\tilde{G}(\boldsymbol{k})$ is the Fourier transform of $G(\boldsymbol{r})$. Note that the terms in the square brackets in Eq. (33) are contributions from the individual displacements (i.e., $G(\boldsymbol{0})$), and these terms are identical to the right-hand side of Eq. (28) for small $|\boldsymbol{k}|$ because $|\boldsymbol{k}|^2 G(\boldsymbol{0}) = |\boldsymbol{k}|^2 \left\langle |\boldsymbol{u}|^2 \right\rangle / d \approx 1 - \left|\tilde{f}_1(\boldsymbol{k})\right|^2$ in the same regime. The rest terms in Eq. (33) are contributions from "correlations" in displacements.

Remarks:

1. *Correlated* perturbed lattices are different from *uncorrelated* ones in two respects; (a) Bragg peaks and (b) existence of nonhyperuniform states. Both types of perturbed lattices have Bragg peaks that are centered at the same positions of their progenitor lattices. While correlated perturbed lattices have broadened peaks as thermalized crystals do, uncorrelated ones have peaks that are not broadened but weakened compared to those in the initial lattice.

2. In contrast to uncorrelated perturbed lattices that are always hyperuniform, correlated ones can be nonhyperuniform. Suppose that for a perturbed lattice in $\mathbb{R}^d$, the function $\tilde{G}(\boldsymbol{k})$, which is given in Eq. (33), exhibits the power-law behavior $\tilde{G}(\boldsymbol{k}) \sim |\boldsymbol{k}|^\beta$ for small $|\boldsymbol{k}|$. It follows that the perturbed lattice is no longer hyperuniform when $\beta = -2$, i.e.,

$$\tilde{G}(\boldsymbol{k}) \sim |\boldsymbol{k}|^{-2} \quad (|\boldsymbol{k}| \ll 1), \tag{34}$$

because the term $|\boldsymbol{k}|^2 \tilde{G}(\boldsymbol{k})$ in Eq. (33) converges to a positive constant as $|\boldsymbol{k}| \to 0$. For low dimensional perturbed lattices ($d \leq 2$), this condition implies that the variance $\left\langle |\boldsymbol{u}|^2 \right\rangle$ becomes infinite.

B. Class III Hyperuniformity

Class III (hyperuniform) point processes are characterized by the exponent $0 < \alpha < 1$ in the large-R behavior of the number variance $\sigma_N^2(R)$, or equivalently, in the small-wavenumber behavior of $S(\boldsymbol{k})$; see Eq. (12). A few class III systems have been reported, e.g., critical absorbing states of random organization models ($\alpha \approx 0.45$ ($d = 1$) and 0.425 ($d = 2$)) [30] and some classical ground states generated by the collective coordinates optimization techniques [14, 48]. However, as noted in Sec. IV A, one can generate class III perturbed lattices with $0 < \alpha < 1$. Moreover, in the construction of class III systems, generating uncorrelated perturbed lattices is computationally advantageous over other methods, e.g., the collective coordinate optimization technique [14, 48] and random organization models [30, 33], in two respects: (a) parallelization is straightforward, and (b) the computational cost is in the order of particle number N.

To generate d-dimensional class III perturbed lattices, the singlet probability density should have a power-law tail, i.e., $f_1(\boldsymbol{u}) \sim |\boldsymbol{u}|^{-(d+\alpha)}$ as $|\boldsymbol{u}| \to \infty$ and $0 < \alpha < 1$ [60, 80]. The α-stable distributions [81] are one-dimensional examples of such singlet densities, but it is difficult to implement them since they can only be analytically expressed in terms of their characteristic functions.

Here, we will present one of the simplest singlet density functions to generate class III perturbed lattices in $\mathbb{R}^d$:

$$f_1(\boldsymbol{r};\delta,\alpha) \equiv \begin{cases} K(d,\alpha,\delta)\,, & |\boldsymbol{r}| \leq \delta \\ K(d,\alpha,\delta)\,(|\boldsymbol{r}|/\delta)^{-d-\alpha}\,, & |\boldsymbol{r}| > \delta, \end{cases} \tag{35}$$

where the normalization constant is given by $K(d,\alpha,\delta) = \frac{\Gamma(1+d/2)\alpha}{\pi^{d/2}(d+\alpha)\delta^d}$, and two parameters: an exponent $\alpha \in (0,1)$ and a characteristic length scale $\delta \in (0,\infty)$. Expressions for the cumulative distribution, its inverse and the characteristic function of $f_1(\boldsymbol{r};\delta,\alpha)$ are provided in Appendix

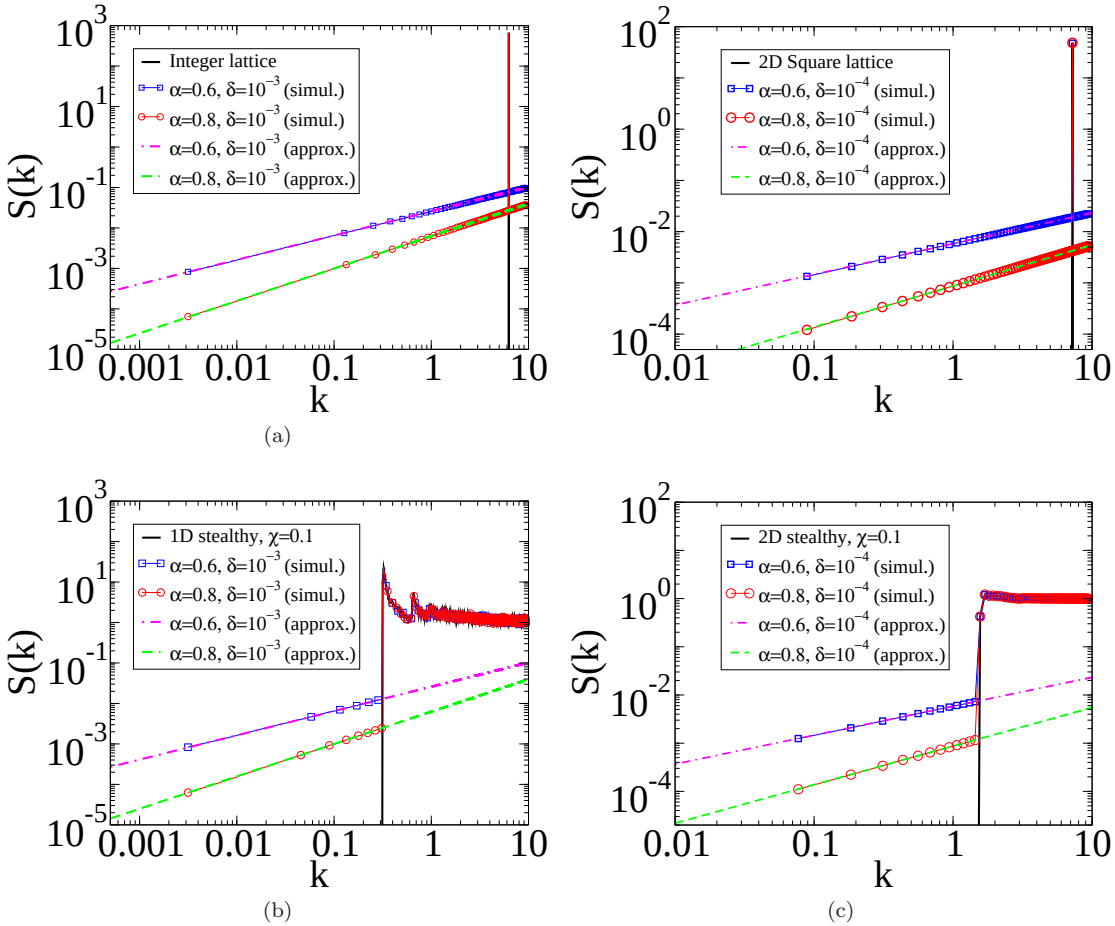

FIG. 4. Log-log plots of approximation and numerical results for structure factors of perturbed point configurations, which are generated by stochastically displacing each particle by the singlet distribution $f_1(\boldsymbol{u};\delta,\alpha)$ defined in Eq. (35). Initial configurations include the following: (a) the integer lattice for $d=1$, (b) the square lattice for $d=2$, and (c)-(d) stealthy disordered hyperuniform point configurations with $\chi=0.1$ ($d=1,2$ for (c) and (d), respectively). A black solid line in each panel shows $S_0(k)$ of the initial configurations.

A. We note that this method can be applied to any class I system to obtain class III systems; see Fig. 4(c) and (d) for examples.

Substituting the characteristic function (A5) into Eq. (28), we obtain the small-$|\boldsymbol{k}|$ asymptotic behavior of $S(k)$ for an uncorrelated perturbed point process via the singlet density (35):

$$S(k) = 2\,A(d,\alpha)\left(\frac{k\delta}{2}\right)^{\alpha} + \mathcal{O}\Big(k^{\min\{2\alpha,2\}}\Big) \qquad (|k\delta| \ll 1), \tag{36}$$

where $k \equiv |\boldsymbol{k}|$ and $A(d,\alpha)$ is defined as

$$A(d,\alpha) \equiv \Gamma(1+d/2)\Gamma(1-\alpha/2)/\Gamma(1+(d+\alpha)/2). \tag{37}$$

As shown in Fig. 4, our approximation formula (36) is in excellent agreement with numerical simulations of $S(k)$.

Large system size is necessary to observe the class III behavior in $S(k)$ because this behavior results from large displacements. Suppose that an initial point configuration lay in a d-dimensional periodic hypercubic box of side length L. Then, one can estimate the relative error ϵ in the approximation (36) at the lowest wavenumber $\underline{k} = 2\pi/L$ by comparing terms in series expansion of $S(k)$ about $k=0$. We find the lower bound $L_{\min}$ of system size as follows:

$$L > L_{\min} \equiv \frac{2\pi}{\underline{k}} = \pi\delta\left(\frac{A(d,\alpha)}{2\epsilon}\right)^{1/\alpha}, \tag{38}$$

ignoring statistical uncertainties that also increase as wavenumber decreases.

Remarks:

1. The singlet function (35) can be used to generate class II perturbed lattices by setting $\alpha = 1$.

2. We generate 100 initial configurations at unit number density for each system. Initial point configurations have particles of $N = 2\times10^3$ ($d=1$) or $N = 10^4$ ($d=2$). Subsequently, we generate 10^2 perturbed configurations from each initial configuration via a singlet function $f_1(\boldsymbol{u};\delta,\alpha)$, given in

Eq. (35), using parameters in Fig. 4. The computed structure factors are presented in Fig. 4.

3. Taking the relative error to be $\epsilon = 10^{-3}$, some lower bounds of system size $L_{\min}$, calculated from Eq. (38), are listed in Table I.

TABLE I. Smallest system sizes $L_{\min}$ that correspond to parameter sets, shown in Fig. 4.

	$\alpha = 0.8$	$\alpha = 0.6$
$d = 1,\ \delta = 10^{-3},\ L = 2 \times 10^3$	1.1×10	1.4×10^2
$d = 2,\ \delta = 10^{-4},\ L = 10^2$	9.3×10^{-1}	1.2×10

V. EFFECT OF PHONON MODES

Previously, Torquato *et al.* [16] theoretically and numerically showed that disordered stealthy hyperuniform ground states become nonhyperuniform in proportion to the temperature (i.e., $S(0) \propto T$) for sufficiently low T. In this study, however, the small-wavenumber behavior of $S(\boldsymbol{k})$ was not obtained, and the theoretical prediction was derived from the compressibility relation (13) without considering the underlying mechanisms. In this section, we investigate the mechanisms associated with thermal excitations that destroy the hyperuniformity of ground states, whether they are disordered or not, and obtain a corresponding predictive formula for the structure factor $S(\boldsymbol{k})$ for small wavenumbers. For simplicity, we focus on thermal excitations (phonon modes) in classical crystalline solids for sufficiently low temperatures.

Consider a ground-state crystal at $T = 0$, which is necessarily hyperuniform and indeed stealthy [1, 16], meaning that $S(\boldsymbol{k}) = 0$ up to the first Bragg-peak wavenumber. Now, imagine gradually increasing the temperature. One might surmise that each particle symmetrically moves around its equilibrium position, and thus the averaged positions of the particles over a long period of time would be identical to the ideal crystalline structure. This scenario would lead one to falsely conclude that *thermalized* crystals (crystals in thermal equilibrium) are hyperuniform.

Thermalized crystals have been extensively investigated in fields of solid-state physics and crystallography. In solid-state physics, there are two important (quantum mechanical) models for harmonic crystals, i.e., *Einstein* and *Debye* solids; see Fig. 5. Roughly speaking, in an Einstein solid, constituent particles behave as independent harmonic oscillators. In a Debye solid, collective motions of the particles arise as elastic waves, each mode of which behaves like an independent oscillator, called a *phonon*. It is noteworthy that Einstein and Debye solids can be mapped to uncorrelated and correlated perturbed lattices, respectively. Thus, an Einstein solid, which corresponds to the aforementioned scenario, cannot be nonhyperuniform at a positive temperature, and we focus on Debye solids.

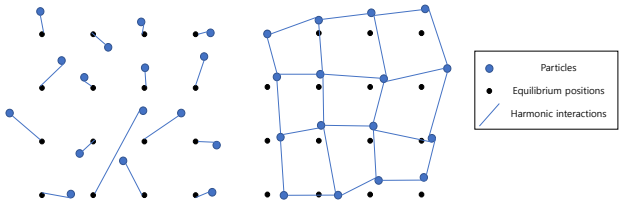

FIG. 5. Schematics illustrating particle displacements in Einstein (left) and Debye solids (right) at a positive temperature. For illustrative purposes, displacements are exaggerated. The particles (large blue dots) in an Einstein solid 'independently' experience harmonic restoring interactions (blue line) toward their equilibrium positions. By contrast, the particles in a Debye solid interact with their nearest neighbors. In summary, displacements in Einstein and Debye solids are uncorrelated and correlated, respectively, leading to different behaviors in long-wavelength density fluctuations.

In crystallography, it has been known that thermally excited elastic waves (phonons) in crystals cause background scattering, called *thermal diffuse scattering*. In the past, this subject had been extensively studied by utilizing approximations for $\hat{\phi}(\boldsymbol{k}; \boldsymbol{r})$, which is given in Eq. (27). For instance, the well-known *Debye-Waller factor* [40], $\exp\Big(-\Big\langle(\boldsymbol{q}\cdot\boldsymbol{u})^2\Big\rangle\Big)$ is essentially a higher-order expression of the quantity $1 - \sum_{\mu,\nu=1}^{d} k_\mu k_\nu\, G_{\mu\nu}(\boldsymbol{0})$ in Eq. (32). However, heretofore, a quantitative description of the small-wavenumber behavior of the structure factor of a thermalized crystal in the harmonic regime has been lacking. This is partly because previous studies have mainly focused on diffuse scattering near Bragg peaks rather than the small-wavenumber behavior. Furthermore, many previous theoretical predictions become invalid for low-dimensional crystals ($d \le 2$) because they contain the Debye-Waller factor that vanishes at any positive temperature for these cases [40, 82].

Our objective here is to derive an explicit expression for the structure factor of classical Debye solids within the harmonic regime, especially in the vicinity of $\boldsymbol{k} = \boldsymbol{0}$. In order to formulate a predictive theory for low dimensions, we avoid starting from standard formulas with the accompanying Debye-Waller factor.

A. Simple Harmonic Lattices

In the harmonic approximation, the potential energy $\Phi(\{\boldsymbol{R}\})$ of crystalline solids can be described as [40, 42, 83]: $\Phi(\{\boldsymbol{R}\}) \approx \frac{1}{2}\sum_{\boldsymbol{R},\boldsymbol{R}'} u_\mu(\boldsymbol{R})\, D_{\mu\nu}(\boldsymbol{R}-\boldsymbol{R}')\, u_\nu(\boldsymbol{R}')$, where $u_\nu(\boldsymbol{R})$ represents the ν-component of displacement vector $\boldsymbol{u}(\boldsymbol{R})$ of a particle whose equilibrium position is $\boldsymbol{R}$, and $D_{\mu\nu}(\mathbf{R})$ is called the dynamical matrix.

Suppose a finite subset $\Lambda(L)$ of an infinitely large Bravais lattice in $\mathbb{R}^d$, which contains $N = L^d$ particles. Un-

der periodic boundary conditions, motion of a particle at $\boldsymbol{R}$ can be described by a superposition of *normal modes* $\tilde{\boldsymbol{u}}_s(\boldsymbol{q},t)\,e^{i\boldsymbol{q}\cdot\boldsymbol{R}}$, i.e.,

$$\boldsymbol{u}(\boldsymbol{R},t)=\frac{1}{\sqrt{N}}\sum_{\boldsymbol{q},s}\tilde{\boldsymbol{u}}_s(\boldsymbol{q},t)\,e^{i\boldsymbol{q}\cdot\boldsymbol{R}}, \tag{39}$$

where a normal coordinate $\tilde{\boldsymbol{u}}_s(\boldsymbol{q},t)\equiv\tilde{u}_s(\boldsymbol{q})\,\hat{\boldsymbol{\epsilon}}_s(\boldsymbol{q})\,e^{i\omega_s(\boldsymbol{q})t}$ represents elastic wave characterized by a wavevector $\boldsymbol{q}$, polarization $\hat{\boldsymbol{\epsilon}}_s(\boldsymbol{q})$, and angular frequency $\omega_s(\boldsymbol{q})$. We use the shorthand notation $\sum_{\boldsymbol{q},s}\equiv\sum_{\boldsymbol{q}\in\Lambda_1^*(L)}\sum_{s=1}^{d}$, where $\Lambda_1^*(L)$ denotes the first Brillouin zone of $\Lambda(L)$. Note that a normal coordinate is essentially a spatial Fourier component of $\boldsymbol{u}(\boldsymbol{R},t)$.

The quantities $\hat{\boldsymbol{\epsilon}}_s(\boldsymbol{q})$ and $\omega_s(\boldsymbol{q})$ can be determined by solving the following eigenvalue problem;

$$m\,{\omega_s}^2(\boldsymbol{q})\,\hat{\epsilon}_s^{\mu}(\boldsymbol{q})=\sum_{\nu=1}^{d}\tilde{D}_{\mu\nu}(\boldsymbol{q})\,\hat{\epsilon}_s^{\nu}(\boldsymbol{q}), \tag{40}$$

where $\hat{\epsilon}_s^{\nu}(\boldsymbol{q})$ is the ν-component of $\hat{\boldsymbol{\epsilon}}_s(\boldsymbol{q})$, m is the mass of a single particle and $\tilde{D}_{\mu\nu}(\boldsymbol{q})$ is the Fourier transform of the dynamical matrix $D_{\mu\nu}(\boldsymbol{R})$. Thus, for each wavevector $\boldsymbol{q}$, there are d independent normal modes, and their polarization vectors $\hat{\boldsymbol{\epsilon}}_s(\boldsymbol{q})$ satisfy the orthogonality (41) and closure (42) relations [83];

$$\hat{\boldsymbol{\epsilon}}_s(\boldsymbol{q})\cdot\hat{\boldsymbol{\epsilon}}_{s'}(\boldsymbol{q})=\delta_{s,s'} \tag{41}$$

$$\sum_{s=1}^{d}\hat{\epsilon}_s^{\mu}(\boldsymbol{q})\,\hat{\epsilon}_s^{\nu}(\boldsymbol{q})=\delta_{\mu,\nu}, \tag{42}$$

where $\delta_{s,s'}$ is the Kronecker delta symbol. Using the normal coordinates (39) and the relation (40), total energy E of a harmonic crystal can be decomposed into a sum of elastic and kinetic energy of each normal mode:

$$E=\sum_{\boldsymbol{q},s}\left[\frac{1}{2}m\,{\omega_s}^2(\boldsymbol{q})\,|\tilde{\boldsymbol{u}}_s(\boldsymbol{q},t)|^2+\frac{1}{2}m\left|\frac{\partial\tilde{\boldsymbol{u}}_s}{\partial t}(\boldsymbol{q},t)\right|^2\right]. \tag{43}$$

In Sec. V, we will consider a d-dimensional simple cubic lattice where each particle is connected to its nearest neighbors by springs of spring constant K. The potential energy of this system is approximately given as

$$\Phi_{\text{cubic}}\approx\frac{K}{2}\sum_{\langle\boldsymbol{R},\boldsymbol{R}'\rangle}|\boldsymbol{u}(\boldsymbol{R})-\boldsymbol{u}(\boldsymbol{R}')|^2, \tag{44}$$

where $\langle\boldsymbol{R},\boldsymbol{R}'\rangle$ indicates that two sites $\boldsymbol{R}$ and $\boldsymbol{R}'$ are nearest neighbors. Its dynamical matrix is given by $D_{\mu\nu}(\boldsymbol{R})=\delta_{\mu,\nu}K\sum_{\langle\boldsymbol{R}',\boldsymbol{0}\rangle}(\delta_{\boldsymbol{R},\boldsymbol{0}}-\delta_{\boldsymbol{R},\boldsymbol{R}'})$, and its Fourier transform is

$$\tilde{D}_{\mu\nu}(\boldsymbol{k})=\delta_{\mu,\nu}4K\sum_{i=1}^{d}\sin^2(k_ia/2), \tag{45}$$

where a is the lattice constant. Using (40) and (45), one can obtain the degenerate dispersion relations:

$$\omega^2(\boldsymbol{k})=\frac{4K}{m}\sum_{i=1}^{d}\sin^2(k_ia/2), \tag{46}$$

regardless of polarization s. For small $|\boldsymbol{k}|$, one obtains a linear dispersion relation:

$$\omega(\boldsymbol{k})=c\,|\boldsymbol{k}|+\mathcal{O}\Big(|\boldsymbol{k}|^2\Big), \tag{47}$$

where c is the sound speed in the continuum limit ($|\boldsymbol{k}|\to 0$), given by $c\equiv\sqrt{Ka^2/m}$. Here, the speed sound c is independent of the polarization, but in general it depends on the polarization. In Appendix C, we derive an isotropic expression of (46) as follows:

$$\omega^2(k)\approx(ck)^2\left(1-\frac{(ka)^2}{4(d+2)}\right). \tag{48}$$

B. Static Structure Factor of Thermalized Crystals

We will consider a finite subset $\Lambda(L)$ of a d-dimensional Bravais lattice of unit lattice constant, as described in Sec. V A, and assume the classical harmonic interactions. We first present a heuristic derivation of the small-wavenumber behavior of the structure factor at low temperatures [84]. The rigorous derivation that leads to the same result is provided in Appendix B.

The collective coordinates can be approximated for small displacements by

$$\begin{aligned}\tilde{n}(\boldsymbol{k})&=\sum_{\boldsymbol{R}}\exp(-i\boldsymbol{k}\cdot\boldsymbol{R})\exp(-i\boldsymbol{k}\cdot\boldsymbol{u}(\boldsymbol{R},t))\\&\approx\sum_{\boldsymbol{R}}\exp(-i\boldsymbol{k}\cdot\boldsymbol{R})\Big[1-i\boldsymbol{k}\cdot\boldsymbol{u}(\boldsymbol{R},t)\Big]\\&=\left[\sum_{\boldsymbol{R}}\exp(-i\boldsymbol{k}\cdot\boldsymbol{R})\right]-i\sqrt{N}\boldsymbol{k}\cdot\tilde{\boldsymbol{u}}(\boldsymbol{k},t),\end{aligned} \tag{49}$$

where we use the fact that normal coordinates $\tilde{\boldsymbol{u}}(\boldsymbol{k},t)$ are the Fourier components of displacement vectors $\boldsymbol{u}(\boldsymbol{R},t)$. Here, we note that for small $|\boldsymbol{k}|$, the quantity $\sum_{\boldsymbol{R}}\exp(-i\boldsymbol{k}\cdot\boldsymbol{R})$ is zero in this regime because an ideal lattice is stealthy hyperuniform. Thus, the structure factor of harmonic crystals can be approximately given by

$$S(\boldsymbol{k})=\lim_{N\to\infty}\frac{1}{N}\Big\langle|\tilde{n}(\boldsymbol{k})|^2\Big\rangle\approx\Big\langle|\boldsymbol{k}\cdot\tilde{\boldsymbol{u}}(\boldsymbol{k},t)|^2\Big\rangle, \tag{50}$$

for $0<|\boldsymbol{k}|\ll 1$. In fact, for low-dimensional crystals ($d\le 2$), the approximation used in Eq. (49) is not justifiable because the quantity $\Big\langle|\boldsymbol{u}|^2\Big\rangle$ diverges in the thermodynamic limit [82]. Nonetheless, it is noteworthy that the result (50) is identical to the one rigorously derived in Appendix B.

According to the equipartition theorem, the ensemble average of potential energy (43) of a normal mode with a polarization index s is expressed as

$$\frac{1}{2}m\,{\omega_s}^2(\boldsymbol{k})\left\langle|\tilde{\boldsymbol{u}}_s(\boldsymbol{k},t)|^2\right\rangle=\frac{1}{2}k_BT,\quad s=\|,2,\cdots,d,\ (51)$$

where the index $\|$ indicates the longitudinal polarization at a given wavevector $\boldsymbol{k}$ and m is the mass of a single particle. Thus, the expression (50) can be simplified as [61]

$$S(\boldsymbol{k})=\frac{|\boldsymbol{k}|^2}{m\,{\omega_\|}^2(\boldsymbol{k})}k_BT.\qquad(52)$$

For the hypercubic model described in Sec. V A, we obtain the small-wavenumber expression for the isotropic structure factor $S(|\boldsymbol{k}|)$ by substituting the dispersion relation (48) into Eq. (52):

$$S(|\boldsymbol{k}|)=\overline{T}\left[1+\frac{(|\boldsymbol{k}|\,a)^2}{4(d+2)}\right]+\mathcal{O}\Big(|\boldsymbol{k}|^4\Big),\qquad(53)$$

where a is the lattice constant and $\overline{T}$ is a dimensionless temperature, defined as

$$\overline{T}\equiv k_BT/(mc^2).\qquad(54)$$

Our approximate result (53) is consistent with numerical simulations for spatial dimensions $d=1,2,3$: see Fig. 6. Taking the limit $|\boldsymbol{k}|\to 0$ in Eq. (53) and comparing to the compressibility relation (13) enables us to determine the isothermal compressibility explicitly:

$$\kappa_T=(Ka^{2-d})^{-1},\qquad(55)$$

which is identical to the inverse of the bulk modulus for the corresponding spring networks.

Expression (50) implies that only *sound waves* (longitudinal elastic waves) contribute to long-wavelength density fluctuations or nonhyperuniformity of thermalized crystals. It is reasonable because while sound waves are caused by density modulations, transverse waves result from volume-preserving shear deformations. In addition, the predicted hyperuniformity of an "incompressible" system in thermal equilibrium would result from a non-relativistic (infinite) speed of sound. The reader is referred to a recent study on a perfect glass model that is hyperuniform and has the same attribute of a non-relativistic (infinite) speed of sound [85].

For a non-Bravais crystal of N_b basis atoms, there are N_b independent "longitudinal" normal modes at each wavevector $\boldsymbol{k}$ [40], and thus Eq. (52) will be modified as

$$S(\boldsymbol{k})=\sum_{i=1}^{N_b}\frac{|\boldsymbol{k}|^2}{\mu_i\,{\omega_{\|(i)}}^2(\boldsymbol{k})}k_BT,\qquad(56)$$

where μ_i are some finite constants of mass unit, and $\omega_{\|(i)}(\boldsymbol{k})$ is the angular frequency of ith longitudinal normal mode. In the *acoustic mode* ($i=1$), all basis atoms in the same unit cell move *in phase*, while in *optical modes* ($i=2,\cdots,N_b$), the basis atoms move *out of phase*. For small wavenumbers, only acoustic modes have linear dispersion relations, as in (47), while optical modes have non-linear ones, i.e., $\lim_{|\boldsymbol{k}|\to 0}\omega_{\|(i)}(\boldsymbol{k})\neq 0$. Therefore, in the limit of $|\boldsymbol{k}|\to 0$, it is only the "longitudinal acoustic modes" that can contribute to the long-wavelength density fluctuations, i.e., $S(\boldsymbol{0})=\frac{K_BT}{\mu_1c_1^2}$, where $c_1\equiv\lim_{|\boldsymbol{k}|\to 0}\omega_{\|(1)}(\boldsymbol{k})/|\boldsymbol{k}|$.

Since thermalized crystals at a positive temperature can be mapped to "nonhyperuniform" perturbed lattices, their displacement-displacement correlation function $G_{\mu\nu}(\boldsymbol{r})$ satisfies the condition (34). Indeed, the simple harmonic crystal model in $\mathbb{R}^d$ satisfies consistently the condition as follows:

$$\tilde{G}_{\mu\nu}(\boldsymbol{k})\approx\delta_{\mu,\nu}\frac{\overline{T}}{|\boldsymbol{k}|^2}\quad(|\boldsymbol{k}|\,a\ll 1),\qquad(57)$$

where $\overline{T}$ is defined by Eq. (54) and a detailed derivation is provided in Appendix D. Here, we note that since $\left\langle|\boldsymbol{u}|^2\right\rangle/d=G(\boldsymbol{0})$, the asymptotic relation (57) implies that the variance in displacements $\left\langle|\boldsymbol{u}|^2\right\rangle$ diverge, or equivalently, the Debye-Waller factor [82] vanishes for low dimensional crystals.

Remarks:

1. Equilibrium hard-sphere systems in $\mathbb{R}^3$ exhibits the same structure factor scaling as in (53) as they approach to the FCC jamming point along the stable crystal branch [86]. This behavior is attributed to collective "vibrational" motions due to collisions, which are the hard-sphere analogs of phonons in systems of particles interacting with continuous pair potentials.

2. The selection rule $\sum_{\boldsymbol{Q}}\delta\Big(-\boldsymbol{k}+\sum_{\boldsymbol{q},s}\boldsymbol{q}(z(\boldsymbol{q},s)+z'(\boldsymbol{q},s)),\boldsymbol{Q}\Big)$ in Eq. (B5) can be interpreted as the crystal momentum conservation [40]. Then, the result (50) corresponds to the single-phonon scattering.

3. To gain some physical idea of the dimensionless temperature $\overline{T}$, we provide estimations of a melting point T_M and Debye temperature T_D [40] in the unit of $\overline{T}$. To estimate the order of magnitude of T_M, we use the Lindemann criterion [40, 87] that $\left\langle|\boldsymbol{u}|^2\right\rangle\approx(c_la)^2$ near T_M, where a is the lattice constant and $c_l\approx 0.1$. In $d=3$, $\overline{T}_M\sim 10^{-2}$ and $\overline{T}_D\sim 10^{-3}$, which are consistent with experimental data for many solids; see Table III. In numerical simulations, temperatures are much lower than the melting point, i.e., $\overline{T}\leq 0.01\overline{T}_M$. We note that for the illustrative purposes, a thermalized lattice in Fig. 1 is set to be at an exceedingly high temperature $\overline{T}=0.05$.

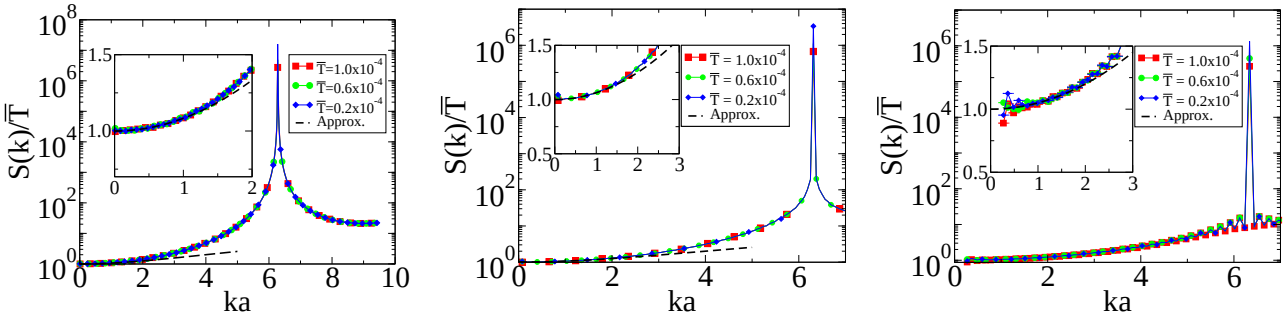

FIG. 6. Semi-log plots of approximate and numerical results for structure factors for thermalized hypercubic lattices calculated from the Monte Carlo technique; (a) $d = 1$, (b) $d = 2$, and (c) $d = 3$. Note that structure factors are normalized by the dimensionless temperature $\overline{T}$ defined by the relation (54). The approximate results are calculated from the formula (53). Insets in each of panels are magnifications in the small-wavenumber regime.

4. We use the simulated-annealing technique to simulate thermalized crystals with the potential energy (44). Each simulation starts from the melting point ($\overline{T} = 0.01$) and then employs an exponential cooling schedule to achieve a target temperature. At each temperature in the cooling schedule, we adjust the maximum displacement of trial moves such that the acceptance rate is around a half. We let the systems evolve for $10\tau_s$ MC cycles before sampling the configurations, and then check whether the acceptance ratio is around a half for the next $\tau_{\rm test}$ MC cycles. Table II lists the sampling parameters for $d = 1, 2$, and 3, respectively.

TABLE II. Parameters used in the Monte Carlo simulations of thermalized crystals in Fig. 6. We sample sequentially $N_{\rm samp}$ configurations in the interval of τ_s MC cycles. For one MC cycle, a single trial movement per one particle is sequentially made.

d	1	2	3
N	1000	100^2	30^3
$N_{\rm samp}$	5×10^4	10^4	10^3
τ_s	5×10^3	10^2	10
$\tau_{\rm test}$	10^3	5×10^2	10^2

5. For a $N \times N$ symmetric positive-definite matrix A, its Gaussian integral has the following property [42]:

$$\langle x_i x_j \rangle \equiv \frac{\int_{\mathbb{R}^N} x_i x_j \exp\left(-\frac{1}{2}\sum_{i,j=1}^N A_{ij} x_i x_j\right) d\boldsymbol{x}}{\int_{\mathbb{R}^N} \exp\left(-\frac{1}{2}\sum_{i,j=1}^N A_{ij} x_i x_j\right) d\boldsymbol{x}} = \left(A^{-1}\right)_{ij},$$

where A^{-1} is the inverse of A. Thus, one immediately obtains an expression equivalent to Eq. (57):

$$\tilde{G}_{\mu\nu}(\boldsymbol{k}) \equiv \langle \tilde{u}_\mu(\boldsymbol{k}, t)\, \tilde{u}^*_\nu(\boldsymbol{k}, t)\rangle_{\rm th} = (k_B T)\tilde{D}^{-1}_{\mu\nu}(\boldsymbol{k}), \quad (58)$$

where $\tilde{D}^{-1}(\boldsymbol{k})$ is the inverse of the Fourier transform $\tilde{D}(\boldsymbol{k})$ of the dynamical matrix.

VI. DISCUSSIONS AND CONCLUSIONS

In this paper, we have theoretically and numerically investigated the degree to which hyperuniformity is degraded or destroyed due to the presence of imperfections in otherwise perfect hyperuniform point processes. We focused on three types of imperfections, including (1) uncorrelated point defects, (2) stochastic particle displacements, and (3) thermal excitations. We derived explicit formulas for the small-wavenumber behaviors (20), (25), (36), and (52) for the structure factors $S(\boldsymbol{k})$ and showed that these expressions are consistent with numerical simulations in Figs. 2, 3, 4, and 6. These results show that either the violation of the infinite-wavelength criterion (8) or changes in the small-$|\boldsymbol{k}|$ behavior of $S(\boldsymbol{k})$ without violating the condition provides an unambiguous means to detect imperfections in otherwise amorphous hyperuniform systems.

Our results indicate that uncorrelated point defects (vacancies and interstitials) and thermal excitations destroy the hyperuniformity of initial systems, but stochastic displacements can destroy it only when displacements are strongly correlated; see the condition (34). Importantly, we also note that our result (52) provides a direct demonstration that thermal excitations can destroy the hyperuniformity of harmonic crystals, which has been indirectly predicted [16, 39] by the compressibility relation (13).

Note that these results are consistent with the qualitative arguments that we made concerning the several example configurations shown in Fig. 1; specifically, the seemingly more disordered configuration (d) is hyperuniform, but the others (b), (c), and (d) are not. To explain these counterintuitive results, it was helpful to examine the *local number variance* $\sigma^2_N(R)$. In the presence of point defects, as we show in Eqs. (21) and (26), the major contributions in $\sigma^2_N(R)$ come from the variances in the number of point defects contained within a large window. In other words, the tendency of point defects

to cluster, as in the Poisson point process, results in the destruction of hyperuniformity.

Interestingly, as we see in Fig. 1(d), uncorrelated stochastic displacements degrade but cannot destroy the hyperuniformity because particles only near a window boundary can fall in and out of the window in an independent manner, i.e., $\sigma_N^2(R) < R^d$ for large R. Using this property, we presented a simple method to transform class I systems, such as lattices and disordered stealthy hyperuniform systems, to class III systems, defined in Eq. (12), by application of relation (35).

By contrast, correlated stochastic displacements can destroy hyperuniformity in the way that particles near the window boundary move in and out of the window *simultaneously* [88]. Our results (50) and (57) show that for thermalized crystals, long-wavelength "longitudinal acoustic waves" arise such correlated displacements; see Fig. 1(e).

We have studied the effect of each type of imperfection on the small-wavenumber behavior of structure factors for otherwise perfectly hyperuniform systems. It would be interesting to study how multiple types of imperfections simultaneously affect the hyperuniformity. In the reverse direction, it would be also interesting to know the general conditions under which correlated particle displacements in a nonhyperuniform system can lead to a hyperuniform system.

Our work provides the theoretical underpinnings to study the effect of imperfections on the physical properties that depend sensitively on the degree of hyperuniformity of materials. For instance, according to the type of imperfection that is introduced in a "stealthy hyperuniform" system, the system becomes merely "hyperuniform" or even "nonhyperuniform." Thus, imperfections may influence some exotic physical properties associated with the stealthy hyperuniformity, e.g., complete isotropic photonic bandgaps [7, 8, 13], transparency at high densities [9], negative compressibilities [89] and nearly optimal transport properties [12]. For future study, it would be interesting to investigate the degree to which the presence of imperfections in otherwise hyperuniform systems affect their physical properties. Furthermore, one could explore whether it is possible to continuously modulate the degree of imperfections in a hyperuniform material to achieve desired properties.

ACKNOWLEDGMENTS

The authors are very grateful to Ge Zhang for his help in numerical simulations. This work was supported partially by the Materials Research Science and Engineering Center (MRSEC) program of the National Science Foundation under Award Number DMR-1420073.

Appendix A: Mathematical Details of the Singlet Density (35)

In this appendix, we provide explicit formulas for the cumulative distribution function $C(R)$, its inverse $C^{-1}(y)$, and the characteristic function of the singlet density function (35). The cumulative distribution function $C(R;\delta,\alpha)$ is

$$C(R) \equiv \int_{|\boldsymbol{r}|<R} d\boldsymbol{r}\, f_1(\boldsymbol{r};\delta,\alpha) = \begin{cases} \frac{\alpha}{d+\alpha}\left(\frac{R}{\delta}\right)^d, & R \le \delta \\ 1 - \frac{d}{d+\alpha}\left(\frac{R}{\delta}\right)^{-\alpha}, & R > \delta \end{cases}, \tag{A1}$$

and its inverse function $C^{-1}(y)$ is

$$C^{-1}(y) = \begin{cases} \delta\left(y(1+d/\alpha)\right)^{1/d}, & 0 < y \le \alpha/(d+\alpha) \\ \delta\left((1-y)(1+\alpha/d)\right)^{-1/\alpha}, & \alpha/(d+\alpha) \le y < 1. \end{cases} \tag{A2}$$

One can generate a random radius followed by the probability density function (35) by substituting y in (A2) with a uniformly-distributed random number between 0 and 1.

The explicit expression for the characteristic function of Eq. (35) is

$$\begin{aligned} \tilde{f}_1(k;\delta,\alpha) = &-A(d,\alpha)\,(k\delta/2)^\alpha \\ &+ \alpha/(d+\alpha)\,{}_0F_1\Big(;(1+d)/2;-(k\delta/2)^2\Big) \\ &+ d/(d+\alpha)\,{}_1F_2\Big(-\alpha/2;d/2,1-\alpha/2;-(k\delta/2)^2\Big), \end{aligned} \tag{A3}$$

where $k = |\boldsymbol{k}|$, $A(d,\alpha)$ is given in Eq. (37), and the generalized hypergeometric function ${}_pF_q(\{a\};\{b\};x)$ is defined as

$${}_pF_q(\{a\};\{b\};x) = \sum_{P=0}^{\infty} \frac{(a_1)_P \cdots (a_p)_P}{(b_1)_P \cdots (b_q)_P} \frac{x^P}{P!}, \tag{A4}$$

where $(a)_P \equiv \Gamma(a+P)\,/\,\Gamma(a)$. For small k, Taylor series expansion of Eq. (A3) is

$$\tilde{f}_1(k;\delta,\alpha) = 1 - A(d,\alpha)\,(k\delta/2)^\alpha + \mathcal{O}\big(k^2\big). \tag{A5}$$

Appendix B: Rigorous Derivation of Eq. (50)

Suppose a finite subset $\Lambda(L)$ of a d-dimensional infinite large Bravais lattice, as defined in Sec. V A. Using the Jacobi-Anger expansions

$$\exp(ia\cos\theta) = \sum_{z=-\infty}^{\infty} J_z(a)\, e^{iz(\theta+\pi/2)} \tag{B1}$$

$$\exp(ia\sin\theta) = \sum_{z=-\infty}^{\infty} J_z(a)\, e^{iz\theta}, \tag{B2}$$

and normal coordinates (39), the collective coordinates $\tilde{n}(\boldsymbol{k})$ of a thermalized crystal can be written in a Fourier series:

$$\begin{aligned}
\tilde{n}(\boldsymbol{k}) &= \sum_{\boldsymbol{R}} \exp(-i\boldsymbol{k}\cdot(\boldsymbol{R}+\boldsymbol{u}(\boldsymbol{R},t))) \\
&= \sum_{\boldsymbol{R}} e^{-i\boldsymbol{k}\cdot\boldsymbol{R}} \prod_{\boldsymbol{q},s} \exp(ik_{\boldsymbol{q},s}\cos(\boldsymbol{q}\cdot\boldsymbol{R}+\omega_s(\boldsymbol{q})t)) \exp\big(i^2 k_{\boldsymbol{q},s}\sin(\boldsymbol{q}\cdot\boldsymbol{R}+\omega_s(\boldsymbol{q})t)\big) \\
&= \sum_{\boldsymbol{R}} e^{-i\boldsymbol{k}\cdot\boldsymbol{R}} \prod_{\boldsymbol{q},s} \sum_{z_{\boldsymbol{q},s},z'_{\boldsymbol{q},s}=-\infty}^{\infty} J_{z_{\boldsymbol{q},s}}(k_{\boldsymbol{q},s})\, J_{z'_{\boldsymbol{q},s}}(ik_{\boldsymbol{q},s}) \exp\big(i(z_{\boldsymbol{q},s}+z'_{\boldsymbol{q},s})\,(\boldsymbol{q}\cdot\boldsymbol{R}+\omega_s(\boldsymbol{q})t)+iz_{\boldsymbol{q},s}\pi/2\big) \\
&= \sum_{\boldsymbol{R}} e^{-i\boldsymbol{k}\cdot\boldsymbol{R}} \sum_{\{z(\boldsymbol{q},s),z'(\boldsymbol{q},s)\}} \prod_{\boldsymbol{q},s} \Big[J_{z(\boldsymbol{q},s)}(k_{\boldsymbol{q},s})\, J_{z'(\boldsymbol{q},s)}(ik_{\boldsymbol{q},s}) \\
&\qquad \exp(i(z(\boldsymbol{q},s)+z'(\boldsymbol{q},s))\,(\boldsymbol{q}\cdot\boldsymbol{R}+\omega_s(\boldsymbol{q})t)+i\,z(\boldsymbol{q},s)\,\pi/2)\Big],
\end{aligned} \tag{B3}$$

where $J_n(x)$ is the Bessel function of order n and we use the shorthand notation $k_{\boldsymbol{q},s} \equiv -\boldsymbol{k}\cdot\tilde{\boldsymbol{u}}_s(\boldsymbol{q})/\sqrt{N}$. Here, $\sum_{\{z(\boldsymbol{q},s),z'(\boldsymbol{q},s)\}}$ represents a summation over all possible functions $z(\boldsymbol{q},s)$ and $z'(\boldsymbol{q},s)$ from wavevectors in the first Brillouin zone $\Lambda_1^*(L)$ and polarization indices to integers. Separating the products of exponential functions in Eq. (B3), one obtains

$$\begin{aligned}
\tilde{n}(\boldsymbol{k}) = &\sum_{\{z(\boldsymbol{q},s),z'(\boldsymbol{q},s)\}} \left[\prod_{\boldsymbol{q},s} J_{z(\boldsymbol{q},s)}(k_{\boldsymbol{q},s})\, J_{z'(\boldsymbol{q},s)}(ik_{\boldsymbol{q},s})\right] \exp\left(i\sum_{\boldsymbol{q},s}\Big((z(\boldsymbol{q},s)+z'(\boldsymbol{q},s))\,\omega_s(\boldsymbol{q})\,t+\frac{\pi}{2}\,z(\boldsymbol{q},s)\Big)\right) \\
&\times \sum_{\boldsymbol{R}} \exp\left(i\left(-\boldsymbol{k}+\sum_{\boldsymbol{q},s}\boldsymbol{q}(z(\boldsymbol{q},s)+z'(\boldsymbol{q},s))\right)\cdot\boldsymbol{R}\right)
\end{aligned} \tag{B4}$$

$$\begin{aligned}
= &\sum_{\{z(\boldsymbol{q},s),z'(\boldsymbol{q},s)\}} \left[\prod_{\boldsymbol{q},s} J_{z(\boldsymbol{q},s)}(k_{\boldsymbol{q},s})\, J_{z'(\boldsymbol{q},s)}(ik_{\boldsymbol{q},s})\right] \times N\sum_{\boldsymbol{Q}} \delta\left(-\boldsymbol{k}+\sum_{\boldsymbol{q},s}\boldsymbol{q}(z(\boldsymbol{q},s)+z'(\boldsymbol{q},s)),\boldsymbol{Q}\right) \\
&\exp\left(i\sum_{\boldsymbol{q},s}\Big((z(\boldsymbol{q},s)+z'(\boldsymbol{q},s))\,\omega_s(\boldsymbol{q})\,t+\frac{\pi}{2}\,z(\boldsymbol{q},s)\Big)\right),
\end{aligned} \tag{B5}$$

where we used an identity $\sum_{\boldsymbol{R}} e^{i\boldsymbol{k}\cdot\boldsymbol{R}} = N\sum_{\boldsymbol{Q}}\delta(\boldsymbol{k},\boldsymbol{Q})$, and $\sum_{\boldsymbol{R}}$ and $\sum_{\boldsymbol{Q}}$ represent a summation over all lattice vectors $\boldsymbol{R}$ and over all reciprocal lattice vectors $\boldsymbol{Q}$ of the lattice $\{\boldsymbol{R}\}$, respectively. The Kronecker delta symbol is denoted here by $\delta(\boldsymbol{q},\boldsymbol{q}')$.

Note that for small $|\boldsymbol{k}|$ and $|\boldsymbol{q}|$, the arguments in Bessel functions are small, i.e., $k_{\boldsymbol{q},s} = \mathcal{O}\big(\overline{T}/\sqrt{N}\big)$ so that we can use a power series expansion of the Bessel functions (i.e., $|J_n(x)| = (x/2)^n/n! + \mathcal{O}\big(x^{n+2}\big)$ for small x) to approximate the product of Bessel functions in Eq. (B5):

$$\left[\prod_{\boldsymbol{q},s} J_{z(\boldsymbol{q},s)}(k_{\boldsymbol{q},s})\, J_{z'(\boldsymbol{q},s)}(ik_{\boldsymbol{q},s})\right] \propto |\boldsymbol{k}|^{\sum_{\boldsymbol{q},s}\left(|z(\boldsymbol{q},s)|+\left|z'(\boldsymbol{q},s)\right|\right)} \qquad (|\boldsymbol{k}|\to 0). \tag{B6}$$

Combining the selection rule $\sum_{\boldsymbol{Q}}\delta\Big(-\boldsymbol{k}+\sum_{\boldsymbol{q},s}\boldsymbol{q}(z(\boldsymbol{q},s)+z'(\boldsymbol{q},s)),\boldsymbol{Q}\Big)$ in Eqs. (B5) and (B6) implies that the leading order in Eq. (B6) should be the unity; $\sum_{\boldsymbol{q},s}(|z(\boldsymbol{q},s)|+|z'(\boldsymbol{q},s)|) = 1$. Thus, the collective coordinates can be approximated as

$$\begin{aligned}
\tilde{n}(\boldsymbol{k}) &\approx N\sum_{s=1}^{d}\Big[\,(J_1(k_{\boldsymbol{k},s})\,i + J_1(ik_{\boldsymbol{k},s}))\,e^{i\omega_s(\boldsymbol{k})t} + (J_{-1}(k_{-\boldsymbol{k},s})\,(-i) + J_{-1}(ik_{-\boldsymbol{k},s}))\,e^{-i\omega_s(-\boldsymbol{k})t}\Big] \\
&\approx 2N\sum_{s=1}^{d}\frac{ik_{\boldsymbol{k},s}}{2}e^{i\omega_s(\boldsymbol{k})t} = -i\sqrt{N}\boldsymbol{k}\cdot\sum_{s=1}^{d}\tilde{\boldsymbol{u}}_s(\boldsymbol{k})\,e^{i\omega_s(\boldsymbol{k})t} \\
&= -i\sqrt{N}\boldsymbol{k}\cdot\tilde{\boldsymbol{u}}(\boldsymbol{k},t)\,.
\end{aligned} \tag{B7}$$

Therefore, the leading-order behavior of the structure factor of a thermalized crystal is written as

$$S(\boldsymbol{k}) \equiv \langle\mathcal{S}(\boldsymbol{k})\rangle = \lim_{N\to\infty}\frac{1}{N}\left\langle|\tilde{n}(\boldsymbol{k})|^2\right\rangle \approx \left\langle|\boldsymbol{k}\cdot\tilde{\boldsymbol{u}}(\boldsymbol{k},t)|^2\right\rangle \quad (0<|\boldsymbol{k}|\,a\ll 1). \tag{B8}$$

Appendix C: Derivation of an Isotropic Dispersion Relation (48)

In this appendix, we derive an isotropic dispersion relation (48). Starting from the second-order power series of the exact dispersion relation (46):

$$\omega^2(\boldsymbol{k}) = c^2\,|\boldsymbol{k}|^2\left(1-\frac{(|\boldsymbol{k}|\,a)^2}{12}\sum_{i=1}^{d}\left(\frac{k_i}{|\boldsymbol{k}|}\right)^4\right)+\mathcal{O}\Big(|\boldsymbol{k}|^6\Big), \tag{C1}$$

we will obtain its average over the orientations of $\boldsymbol{k}$. Its orientational average simplifies as

$$\omega^2(k) = (ck)^2\left(1-d/12\left\langle {x_1}^4\right\rangle_{\rm ang}\right)+\mathcal{O}\big(k^6\big), \tag{C2}$$

where $k\equiv|\boldsymbol{k}|$, x_i is the first component of a unit vector $\boldsymbol{x}$, $\left\langle {x_i}^4\right\rangle_{\rm ang}\equiv\oint_{|\boldsymbol{x}|=1}d\boldsymbol{x}\,{x_i}^4/S_d(1)$, and $S_d(1)=2\pi^{d/2}/\Gamma(d/2)$ is the surface area of d-dimensional sphere of unit radius. Here, we use the fact that $\left\langle {x_i}^4\right\rangle_{\rm ang}$ are identical for $i=1,\cdots,d$ due to the rotational symmetry.

In d-dimensional spherical coordinates $\phi\in[0,2\pi]$ and $\theta_j\in[0,\pi]$ for $j=1,\cdots,d-2$, the Cartesian coordinates of a unit vector $\boldsymbol{x}$ are expressed as

$$x_i=\begin{cases}\cos\phi\prod_{j=1}^{d-2}\sin\theta_j, & i=1\\ \sin\phi\prod_{j=1}^{d-2}\sin\theta_j, & i=2\\ \cos\theta_{i-2}\prod_{j=1}^{i-3}\sin\theta_j, & i=3,\cdots,d.\end{cases} \tag{C3}$$

The infinitesimal area dS of the spherical shell of unit radius is written as

$$dS = d\phi\prod_{i=1}^{d-2}\Big[d\theta_i\sin(\theta_i)^{d-i-1}\Big]. \tag{C4}$$

Using the following identity

$$\int_0^\pi dx\sin^m x=\sqrt{\pi}\frac{\Gamma((m+1)/2)}{\Gamma((m+2)/2)}, \tag{C5}$$

one can calculate

$$\begin{aligned}\left\langle {x_1}^4\right\rangle_{\rm ang} &= \frac{1}{S_d(1)}\int_0^{2\pi}d\phi\cos^4\phi\prod_{i=1}^{d-2}\left[\int_0^\pi d\theta_i\sin(\theta_i)^{d+3-i}\right]=\frac{\Gamma(d/2)}{2\pi^{d/2}}\frac{3\pi}{4}\prod_{i=1}^{d-2}\left[\sqrt{\pi}\frac{\Gamma\left(\frac{d+4-i}{2}\right)}{\Gamma\left(\frac{d+5-i}{2}\right)}\right]\\ &= \frac{\Gamma(d/2)}{2\pi^{d/2}}\frac{3}{4}\pi^{d/2}\frac{\Gamma\left(\frac{d+4-(d-2)}{2}\right)}{\Gamma\left(\frac{d+5-1}{2}\right)}=\frac{3}{4}\frac{\Gamma(d/2)}{\Gamma(2+d/2)}=\frac{3}{d(d+2)}.\end{aligned} \tag{C6}$$

Thus, Eq. (C2) becomes

$$\omega^2(k)\approx(ck)^2\left(1-\frac{(ka)^2}{4(d+2)}\right). \tag{C7}$$

Appendix D: Displacement-Displacement Correlation Functions of Thermalized Crystals

In this appendix, we derive Eq. (57) in Sec. V B for a classical Debye solid. Since $G_{\mu\nu}(\boldsymbol{r})$ is defined for the complex variables as $G_{\mu\nu}(\boldsymbol{r})\equiv\langle u_\mu(\boldsymbol{r}+\boldsymbol{R},t)\,u_\nu^*(\boldsymbol{R},t)\rangle=\big\langle\langle u_\mu(\boldsymbol{r}+\boldsymbol{R},t)\,u_\nu(\boldsymbol{R},-t)\rangle_{\boldsymbol{R}}\big\rangle_{\rm th}$, we obtain its Fourier transform by using properties of the autocovariance:

$$\begin{aligned}\tilde{G}_{\mu\nu}(\boldsymbol{k}) &= \langle\tilde{u}_\mu(\boldsymbol{k},t)\,\tilde{u}_\nu(-\boldsymbol{k},-t)\rangle_{\rm th}\\ &= \langle\tilde{u}_\mu(\boldsymbol{k},t)\,\tilde{u}_\nu^*(\boldsymbol{k},t)\rangle_{\rm th},\end{aligned} \tag{D1}$$

where $\langle\cdot\rangle_{\boldsymbol{R}}$ means the average over the positions $\boldsymbol{R}$ and, $\langle\cdot\rangle_{\rm th}$ means a canonical ensemble average.

Using normal coordinates (39), Eq. (D1) simplifies as

$$\begin{aligned}\tilde{G}_{\mu\nu}(\boldsymbol{k}) &= \sum_{s,s'=1}^{d}\hat{\epsilon}_s^\mu(\boldsymbol{k})\hat{\epsilon}_{s'}^\nu(\boldsymbol{k})\left\langle\tilde{u}_s(\boldsymbol{k})\,\tilde{u}_{s'}^*(\boldsymbol{k})\,e^{i(\omega_s(\boldsymbol{k})-\omega_{s'}(\boldsymbol{k}))t}\right\rangle_{\rm th}\\ &= \sum_{s=1}^{d}\hat{\epsilon}_s^\mu(\boldsymbol{k})\hat{\epsilon}_s^\nu(\boldsymbol{k})\,\langle\tilde{u}_s(\boldsymbol{k})\,\tilde{u}_s^*(\boldsymbol{k})\rangle_{\rm th},\end{aligned} \tag{D2}$$

where $\hat{\epsilon}_s^\mu(\boldsymbol{k})$ is the μ-component of a unit polarization vector $\hat{\boldsymbol{\epsilon}}_s(\boldsymbol{k})$ and we used the fact that normal coordinates with different polarizations are independent of one another.

Applying the equipartition theorem into Eq. (D2), we obtain the small-$|\boldsymbol{k}|$ behavior of $\tilde{G}_{\mu\nu}(\boldsymbol{k})$:

$$\tilde{G}_{\mu\nu}(\boldsymbol{k}) = \sum_{s=1}^{d}\frac{\hat{\epsilon}_s^\mu(\boldsymbol{k})\hat{\epsilon}_s^\nu(\boldsymbol{k})}{m\,\omega_s^2(\boldsymbol{k})}k_BT \tag{D3}$$

$$\approx\sum_{s=1}^{d}\frac{\hat{\epsilon}_s^\mu(\boldsymbol{k})\hat{\epsilon}_s^\nu(\boldsymbol{k})}{mc^2\,|\boldsymbol{k}|^2}k_BT=\delta_{\mu,\nu}\frac{\overline{T}}{|\boldsymbol{k}|^2}, \tag{D4}$$

where the degenerate dispersion relations (47) for a simple harmonic crystal in $\mathbb{R}^d$ and the closure relation (42) are used in Eq. (D4). Here, $\overline{T}$ is defined in Eq. (54).

TABLE III. Estimations of Debye temperatures T_D and melting points T_M of solids of some elements in the unit of the dimensionless temperature $\overline{T}$ up to two significant figures. The mass and speed sound are denoted by m and c, respectively.

	m[a] (10^{-23}g)	c[b] (10^3m/s)	T_D[a](K)	$[\overline{T}_D]$	T_M[a](K)	$[\overline{T}_M]$		m[a] (10^{-23}g)	c[b] (10^3m/s)	T_D[a](K)	$[\overline{T}_D]$	T_M[a](K)	$[\overline{T}_M]$
Be	1.50	12.9	1000	[0.0056]	1550	[0.0086]	Mg	4.04	5.77	318	[0.0033]	922	[0.0095]
Al	4.48	6.42	394	[0.0029]	933	[0.0070]	Sn(white)	19.7	3.32	170	[0.0011]	505	[0.0032]
Cu	10.6	4.76	315	[0.0018]	1356	[0.0078]	Ag	17.9	3.65	215	[0.0012]	1234	[0.0071]
Au	32.7	3.24	170	[0.00068]	1337	[0.0054]	Zn	10.9	4.21	234	[0.0017]	693	[0.0050]
Mo	15.9	6.25	380	[0.0008]	2890	[0.0064]	W	30.5	5.22	310	[0.0005]	3683	[0.0061]
Fe	9.44	5.00	420	[0.0025]	1808	[0.011]	Ni	9.75	5.04	375	[0.0021]	1726	[0.0096]
Pd	17.7	2.16	275	[0.0046]	1825	[0.031]	Pt	32.4	3.26	230	[0.0009]	2045	[0.0082]

[a] Taken from Ref. [40].
[b] Taken from Ref. [90].

Appendix E: Debye Temperatures and Melting Points of Some Solids

In this appendix, we estimate two quantities $\overline{T}_D \equiv k_B T_D/mc^2$ and $\overline{T}_M \equiv k_B T_M/mc^2$ from experimental data of some solids and list them in Table III. These two quantities correspond to the Debye temperature T_D and melting point T_M, respectively, in the unit of the dimensionless temperature $\overline{T}$, which is defined in Eq. (54).

* torquato@princeton.edu; http://chemlabs.princeton.edu

[1] S. Torquato and F.H. Stillinger, "Local density fluctuations, hyperuniformity, and order metrics," Phys. Rev. E **68**, 041113 (2003).

[2] C.E. Zachary and S. Torquato, "Hyperuniformity in point patterns and two-phase random heterogeneous media," J. Stat. Mech: Theory Exp. **2009**, P12015 (2009).

[3] S. Torquato, "Hyperuniformity and its generalizations," Phys. Rev. E **94**, 022122 (2016).

[4] C. Lin, P.J. Steinhardt, and S. Torquato, "Hyperuniformity variation with quasicrystal local isomorphism class," J. Phys.: Condens. Matter **29**, 204003 (2017).

[5] E.C. Oğuz, J.E.S. Socolar, P.J. Steinhardt, and S. Torquato, "Hyperuniformity of quasicrystals," Phys. Rev. B **95**, 054119 (2017).

[6] C.E. Zachary, Y. Jiao, and S. Torquato, "Hyperuniformity, quasi-long-range correlations, and void-space constraints in maximally random jammed particle packings. I. Polydisperse spheres," Phys. Rev. E **83**, 051308 (2011).

[7] M. Florescu, S. Torquato, and P.J. Steinhardt, "Designer disordered materials with large, complete photonic band gaps," Proc. Natl. Acad. Sci. U.S.A. **106**, 20658–20663 (2009).

[8] M. Florescu, P.J. Steinhardt, and S. Torquato, "Optical cavities and waveguides in hyperuniform disordered photonic solids," Phys. Rev. B **87**, 165116 (2013).

[9] O. Leseur, R. Pierrat, and R. Carminati, "High-density hyperuniform materials can be transparent," Optica **3**, 763–767 (2016).

[10] W. Man, M. Florescu, E.P. Williamson, Y. He, S.R. Hashemizad, B.Y.C. Leung, D.R. Liner, S. Torquato, P.M. Chaikin, and P.J. Steinhardt, "Isotropic band gaps and freeform waveguides observed in hyperuniform disordered photonic solids," Proc. Natl. Acad. Sci. U.S.A. **110**, 15886–15891 (2013).

[11] Q. Le Thien, D. McDermott, C.J.O. Reichhardt, and C. Reichhardt, "Enhanced pinning for vortices in hyperuniform pinning arrays and emergent hyperuniform vortex configurations with quenched disorder," Phys. Rev. B **96**, 094516 (2017).

[12] G. Zhang, F. Stillinger, and S. Torquato, "Transport, geometrical, and topological properties of stealthy disordered hyperuniform two-phase systems," J. Chem. Phys. **145**, 244109 (2016).

[13] L.S. Froufe-Prez, M. Engel, J.J. Senz, and F. Scheffold, "Band gap formation and anderson localization in disordered photonic materials with structural correlations," Proc. Natl. Acad. Sci. U.S.A. **114**, 9570–9574 (2017).

[14] O.U. Uche, F.H. Stillinger, and S. Torquato, "Constraints on collective density variables: Two dimensions," Phys. Rev. E **70**, 046122 (2004).

[15] R.D. Batten, F.H. Stillinger, and S. Torquato, "Classical disordered ground states: Super-ideal gases and stealth and equi-luminous materials," J. Appl. Phys. **104**, 033504 (2008).

[16] S. Torquato, G. Zhang, and F. Stillinger, "Ensemble theory for stealthy hyperuniform disordered ground states," Phys. Rev. X **5**, 021020 (2015).

[17] G. Zhang, F.H. Stillinger, and S. Torquato, "Ground states of stealthy hyperuniform potentials: I. Entropically favored configurations," Phys. Rev. E **92**, 022119 (2015).

[18] G. Zhang, F.H. Stillinger, and S. Torquato, "Ground states of stealthy hyperuniform potentials. II. Stacked-slider phases," Phys. Rev. E **92**, 022120 (2015).

[19] F.J. Dyson, "Statistical theory of the energy levels of complex systems. I," J. Math. Phys. **3**, 140–156 (1962).

[20] B. Jancovici, "Exact results for the two-dimensional one-component plasma," Phys. Rev. Lett. **46**, 386 (1981).

[21] J.L. Lebowitz, "Charge fluctuations in coulomb systems," Phys. Rev. A **27**, 1491 (1983).

[22] E. Lomba, J.J. Weis, and S. Torquato, "Disordered hyperuniformity in two-component nonadditive hard-disk plasmas," Phys. Rev. E **96**, 062126 (2017).

[23] E. Lomba, J.-J. Weis, and S. Torquato, "Disordered multihyperuniformity derived from binary plasmas," Phys. Rev. E **97**, 010102(R) (2018).

[24] A. Scardicchio, C.E. Zachary, and S. Torquato, "Statistical properties of determinantal point processes in high-dimensional euclidean spaces," Phys. Rev. E **79**, 041108 (2009).

[25] R. Feynman and M. Cohen, "Energy spectrum of the excitations in liquid helium," Phys. Rev. **102**, 1189 (1956).

[26] S. Torquato, A. Scardicchio, and C.E. Zachary, "Point processes in arbitrary dimension from fermionic gases, random matrix theory, and number theory," J. Stat. Mech: Theory Exp. **2008**, P11019 (2008).

[27] Y. Jiao and S. Torquato, "Maximally random jammed packings of Platonic solids: Hyperuniform long-range correlations and isostaticity," Phys. Rev. E **84**, 041309 (2011).

[28] L. Berthier, P. Chaudhuri, C. Coulais, O. Dauchot, and P. Sollich, "Suppressed compressibility at large scale in jammed packings of size-disperse spheres," Phys. Rev. Lett. **106**, 120601 (2011).

[29] A. Donev, F.H. Stillinger, and S. Torquato, "Unexpected density fluctuations in jammed disordered sphere packings," Phys. Rev. Lett. **95**, 090604 (2005).

[30] D. Hexner and D. Levine, "Hyperuniformity of Critical Absorbing States," Phys. Rev. Lett. **114**, 110602 (2015).

[31] J.H. Weijs, R. Jeanneret, R. Dreyfus, and D. Bartolo, "Emergent hyperuniformity in periodically driven emulsions," Phys. Rev. Lett. **115**, 108301 (2015).

[32] K.J. Schrenk and D. Frenkel, "Communication: Evidence for non-ergodicity in quiescent states of periodically sheared suspensions," J. Chem. Phys. **143**, 241103 (2015).

[33] E. Tjhung and L. Berthier, "Criticality and correlated dynamics at the irreversibility transition in periodically driven colloidal suspensions," J. Stat. Mech: Theory Exp. **2016**, 033501 (2016).

[34] D. Hexner and D. Levine, "Noise, Diffusion, and Hyperuniformity," Phys. Rev. Lett. **118**, 020601 (2017).

[35] I. Lesanovsky and J.P. Garrahan, "Out-of-equilibrium structures in strongly interacting rydberg gases with dissipation," Phys. Rev. A **90**, 011603 (2014).

[36] Y. Jiao, T. Lau, H. Hatzikirou, M. Meyer-Hermann, C.C. Joseph, and S. Torquato, "Avian photoreceptor patterns represent a disordered hyperuniform solution to a multiscale packing problem," Phys. Rev. E **89**, 022721 (2014).

[37] D. Chen and S. Torquato, "Designing disordered hyperuniform two-phase materials with novel physical properties," Acta Mater. **142**, 152–161 (2018).

[38] H.L. Montgomery, "The pair correlation of zeros of the zeta function," in *Proc. Symp. Pure Math*, Vol. 24 (1973) pp. 181–193.

[39] S. Torquato, "Hyperuniform States of Matter," arXiv:1801.06924 (2018).

[40] N.W. Ashcroft and N.D. Mermin, *Solid state physics* (Brooks/Cole, Cengage Learning, 10 Davis Drive, Belmont, 1976).

[41] C. Kittel, *Introduction to solid state physics*, 8th ed. (Wiley, 2005).

[42] P.M. Chaikin and T.C. Lubensky, *Principles of condensed matter physics* (Cambridge university press, 2000).

[43] G.E. Dieter, *Mechanical metallurgy*, 3rd ed. (McGraw-Hill, New York :, 1986).

[44] J. Kondo, "Resistance minimum in dilute magnetic alloys," Prog. Theor. Phys. **32**, 37–49 (1964).

[45] A.C. Hewson and J. Kondo, "Kondo effect," Scholarpedia **4**, 7529 (2009).

[46] J.E. Socolar, T. Lubensky, and P.J. Steinhardt, "Phonons, phasons, and dislocations in quasicrystals," Phys. Rev. B **34**, 3345 (1986).

[47] O.U. Uche, S. Torquato, and F.H. Stillinger, "Collective coordinate control of density distributions," Phys. Rev. E **74**, 031104 (2006).

[48] C.E. Zachary and S. Torquato, "Anomalous local coordination, density fluctuations, and void statistics in disordered hyperuniform many-particle ground states," Phys. Rev. E **83**, 051133 (2011).

[49] S. Atkinson, G. Zhang, A.B. Hopkins, and S. Torquato, "Critical slowing down and hyperuniformity on approach to jamming," Phys. Rev. E **94**, 012902 (2016).

[50] E. Tjhung and L. Berthier, "Hyperuniform density fluctuations and diverging dynamic correlations in periodically driven colloidal suspensions," Phys. Rev. Lett. **114**, 148301 (2015).

[51] D. Hexner, P.M. Chaikin, and D. Levine, "Enhanced hyperuniformity from random reorganization," Proc. Natl. Acad. Sci. U.S.A. **114**, 4294–4299 (2017).

[52] Z. Ma and S. Torquato, "Random scalar fields and hyperuniformity," J. Appl. Phys. **121**, 244904 (2017).

[53] Rei Kurita and Eric R. Weeks, "Experimental study of random-close-packed colloidal particles," Phys. Rev. E **82**, 011403 (2010).

[54] R. Dreyfus, Y. Xu, T. Still, L.A. Hough, A. Yodh, and S. Torquato, "Diagnosing hyperuniformity in two-dimensional, disordered, jammed packings of soft spheres," Phys. Rev. E **91**, 012302 (2015).

[55] J. Ricouvier, R. Pierrat, R. Carminati, P. Tabeling, and P. Yazhgur, "Optimizing hyperuniformity in self-assembled bidisperse emulsions," Phys. Rev. Lett. **119**, 208001 (2017).

[56] R. Xie, G.G. Long, S.J. Weigand, S.C. Moss, T. Carvalho, S. Roorda, M. Hejna, S. Torquato, and P.J. Steinhardt, "Hyperuniformity in amorphous silicon based on the measurement of the infinite-wavelength limit of the structure factor," Proc. Natl. Acad. Sci. U.S.A. **110**, 13250–13254 (2013).

[57] G. Zito, G. Rusciano, G. Pesce, A. Malafronte, R. Di Girolamo, G. Ausanio, A. Vecchione, and A. Sasso, "Nanoscale engineering of two-dimensional disordered hyperuniform block-copolymer assemblies," Phys. Rev. E **92**, 050601 (2015).

[58] T.R. Welberry, G.H. Miller, and C.E. Carroll, "Paracrystals and growth-disorder models," Acta Crystallogr., Sect. A: Found. Crystallogr. **36**, 921–929 (1980).

[59] A. Gabrielli and S. Torquato, "Voronoi and void statistics for superhomogeneous point processes," Phys. Rev. E **70**, 041105 (2004).

[60] A. Gabrielli, "Point processes and stochastic displacement fields," Phys. Rev. E **70**, 066131 (2004).

[61] As the temperature increases, anharmonic effects would also contribute to the degradation of hyperuniformity in crystalline ground-states.

[62] J.-P. Hansen and I.R. McDonald, *Theory of simple liquids* (Elsevier, 1990).

[63] L. Pietronero, A. Gabrielli, and F.S. Labini, "Statistical physics for cosmic structures," Physica A **306**, 395–401 (2002).

[64] E. Giamello, M. Chiesa, and M.C. Paganini, "Point Defects in Electron Paramagnetic Resonance," in *Defects at Oxide Surfaces*, edited by Jacques Jupille and Geoff Thornton (Springer International Publishing, Cham, 2015) pp. 303–326.

[65] H. Peisl, "Defect properties from X-ray scattering experiments," J. Phys. Colloques **37**, C7–47–C7–53 (1976).

[66] P.H. Dederichs, "The theory of diffuse X-ray scattering and its application to the study of point defects and their clusters," J. Phys. F: Met. Phys. **3**, 471 (1973).

[67] K. Huang, "X-ray reflexions from dilute solid solutions," Proc. R. Soc. London, Ser. A **190**, 102–117 (1947).

[68] A.T. Chieco, R. Dreyfus, and D.J. Durian, "Characterizing pixel and point patterns with a hyperuniformity disorder length," Phys. Rev. E **96**, 032909 (2017).

[69] A. Gabrielli, M. Joyce, and F.S. Labini, "Glass-like universe: Real-space correlation properties of standard cosmological models," Phys. Rev. D **65**, 083523 (2002).

[70] W.J. Stroud and R.P. Millane, "Cylindrically averaged diffraction by distorted lattices," Proc. R. Soc. London, Ser. A **452**, 151–173 (1996).

[71] M. Sodin and B. Tsirelson, "Random complex zeroes, II. Perturbed lattice," Israel J. Math. **152**, 105–124 (2006).

[72] Y. Peres and A. Sly, "Rigidity and tolerance for perturbed lattices," arXiv:1409.4490 (2014).

[73] S. Ghosh and J. Lebowitz, "Number Rigidity in Superhomogeneous Random Point Fields," J. Stat. Phys. **166**, 1016–1027 (2016).

[74] G. Efstathiou, M. Davis, S. White, and C. Frenk, "Numerical techniques for large cosmological N-body simulations," Astrophys. J., Suppl. Ser. **57**, 241–260 (1985).

[75] E. Renshaw, "Two-dimensional Spectral Analysis for Marked Point Processes," Biom. J. **44**, 718–745 (2002).

[76] D.S. Novikov, J.H. Jensen, J.A. Helpern, and E. Fieremans, "Revealing mesoscopic structural universality with diffusion," Proc. Natl. Acad. Sci. U.S.A. **111**, 5088–5093 (2014).

[77] The Cauchy probability distribution function is given by $f_1(x;\delta,\mu) = \left[\pi\delta(1+((x-\mu)/\delta)^2)\right]^{-1}$, where $\delta \in (0,\infty)$ is a length scale and $\mu \in \mathbb{R}$ is the mean. For more details, see A. Papoulis, *Probability, Random Variables, and Stochastic Processes*, 2nd ed. (McGraw-Hill, 1984).

[78] The Pareto probability distribution function has semi-infinite support, i.e., $x \in [0,\infty)$ and is given by $f_1(x;x_m,\alpha) = \Theta(x-x_m)\,\alpha(x_m/x)^{\alpha+1}/x_m$, where $\Theta(x)$ is the Heaviside step function and $\alpha \in (0,\infty)$ is an exponent. For more details, see B.C. Arnold, *Pareto distribution*, 2nd ed. (CRC Press, 2015).

[79] Gabrielli demonstrated class II perturbed lattices for $d = 1$ via the Cauchy distribution; see Ref. [60].

[80] A. Gabrielli, M. Joyce, and S. Torquato, "Tilings of space and superhomogeneous point processes," Phys. Rev. E **77**, 031125 (2008).

[81] J. Nolan, *Stable distributions: models for heavy-tailed data* (Birkhauser New York, 2003).

[82] Y. Imry, "Long-range order in two dimensions," Crit. Rev. Solid State Mater. Sci. **8**, 157–174 (1979).

[83] W. Jones and N.H. March, *Theoretical solid state physics, volume 1: Perfect lattices in Equilibrium*, dover ed. (John Wiley & Sons Ltd., 1973).

[84] This derivation is similar to that used to derive Huang diffuse scattering in Ref. [91].

[85] G. Zhang, F.H. Stillinger, and S. Torquato, "The Perfect Glass Paradigm: Disordered Hyperuniform Glasses Down to Absolute Zero," Sci Rep **6**, 36963 (2016).

[86] S. Atkinson, F.H. Stillinger, and S. Torquato, "Static structural signatures of nearly jammed disordered and ordered hard-sphere packings: Direct correlation function," Phys. Rev. E **94**, 032902 (2016).

[87] X. Zheng and J. Earnshaw, "On the Lindemann criterion in 2D," EPL **41**, 635 (1998).

[88] For the same reason, the local number variance for a cubic lattice in $\mathbb{R}^3$, which is clearly a hyperuniform system, can increase faster than window volume when one uses a *cubic* window that is aligned with the lattice; see J. Kim and S. Torquato, J. Stat. Mech: Theory Exp. **2017**, 013402 (2017).

[89] R.D. Batten, F.H. Stillinger, and S. Torquato, "Interactions leading to disordered ground states and unusual low-temperature behavior," Phys Rev E **80**, 031105 (2009).

[90] David R.L., ed., *CRC Handbook of Chemistry and Physics*, 84th ed. (CRC Press, 2003).

[91] R. Barabash, J. Chung, and M. Thorpe, "Lattice and continuum theories of Huang scattering," J. Phys.: Condens. Matter **11**, 3075 (1999).